BSGF - Earth Sciences Bulletin 2025, 196, 18
© G.R. Noura *et al.*, Published by EDP Sciences 2025
https://doi.org/10.1051/bsgf/2025019

BSGF Earth Sciences Bulletin
Available online at:
www.bsgf.fr

OPEN ACCESS

Mineralogical and geochemical characteristics of the NNW-NNE trending Libiri doleritic dyke swarm of the Paleoproterozoic Liptako basement (West Niger): Genesis and magmatic evolution

Gambo Ranaou Noura[1,*], Lenka Baratoux[2,3], Richard E. Ernst[4], Hafida El Bilali[4], Abdou Latif Abasse Saley[5], Karimou Dia Hantchi[6], Abdou Dodo Bohari[1] and Yacouba Ahmed[1]

[1] Groundwater and Georesources Laboratory, Faculty of science and technology, University of Abdou Moumouni, BP 10662, Niamey, Niger
[2] GET Laboratory, University of Toulouse 3 Paul Sabatier, IRD, CNRS, UMR 5563, Observatory Midi-Pyrénées, 31400 Toulouse, France
[3] Université Félix Houphouët-Boigny Abidjan-Cocody, UFR-STRM, 22 BP 582 Abidjan 22, Côte d'Ivoire
[4] Department of Earth Sciences, Carleton University, Ottawa, ON K1S 5B6, Canada
[5] Ecole des Mines de l'industrie et de la Géologie (EMIG), African Center of Excellence in Mining Environment (CEA_EM-EMIG), BP 732, Niamey, Niger
[6] Université Dan Dicko Dankoulodo, Faculté des Sciences et Techniques, UMR SERMUG, BP 465 Maradi, Niger

Received: 20 February 2025 / Accepted: 25 August 2025 / Publishing online: 7 November 2025

Abstract – The NNW-NNE Libiri doleritic dyke swarm of the Liptako region of West Niger is one of multiple mafic dyke swarms that crosscut the Birimian formations of the Léo-Man shield in the West African Craton. This NNWNNE trending swarm consists of two different groups based on mineralogy and geochemical composition. Both groups have a matching assembly of minerals (ferro-edenite, pyroxene, plagioclase, biotite, apatite, chlorite, grains with granophyric texture and titanomagnetite-ilmenite). In detail Group I dykes have a distinct intergranular texture and some particular minerals (bytownite, pigeonite, clinoenstatite and sanidine) that differ from those in Group II dykes which have a partially preserved ophitic texture and less calcic plagioclases (albite to labradorite). Variation in Mg# and differentiation index (DI) indicate that Group I (Mg# = 55–65, DI = 16.26–20.19) is more primitive in composition than Group II (Mg# = 30–35, DI = 22.82–50.00). REE and other incompatible element values are elevated in Group II compared to Group I, and the REE slopes are parallel one to each other, which suggests that the two groups are co-genetic and that Group II units are more evolved magmas from Group I. The presence of negative Nb and Ta values normalized to primitive mantle in both groups and the La_n/Yb_n (4.73–6.21) ratios suggests that the magma was formed by partial melting of hydrated garnet lherzolite from the lithospheric mantle, modified by interaction with previously metasomatized lithosphere in subduction setting. Alteration minerals such as ferro-edenite, biotite, epidote and chlorite on augite crystal margins indicate later deuteric alteration or low grade late magmatic metamorphism. Petrography and chemistry of a sample SD (Samira Dyke, a sample from the Libiri pit in the Samira gold mine, which was previously dated at 1791 ± 3 Ma and belong to Group II dykes) suggests the entire swarm of NNW-SSE to NNE-SSW trending dykes belong to the Libiri swarm of a plume-generated Large Igneous Province that extends into formerly adjacent Sarmatia (Baltica) and Amazonia.

Keywords: Geochemistry / dykes / Large Igneous Provinces / swarm / Niger / petrography

Résumé – Caractéristiques minéralogiques et géochimiques de l'essaim de dykes doléritiques de Libiri orienté NNO-NNE du Socle Paléoprotérozoïque du Liptako (Ouest-Niger) : Genèse et évolution magmatique. L'essaim de dykes doléritiques de Libiri NNW-NNE de la région du Liptako, à l'ouest du Niger, est l'un des multiples essaims de dykes mafiques qui recoupent les formations birimiennes du bouclier de Léo-Man, dans le Craton Ouest-Africain. Cet essaim d'orientation NNO-NNE, se compose de deux groupes différents sur la base de la minéralogie et de la composition géochimique. Les deux groupes présentent un assemblage correspondant de minéraux (ferro-édénite, pyroxène, plagioclase, biotite, apatite,

*e-mail: nouragambo828@gmail.com

chlorite, grains avec une texture granophyrique et titanomagnétite-ilménite). En détail, les dykes du groupe I présentent une texture intergranulaire distincte et certains minéraux particuliers (bytownite, pigeonite, clinoenstatite et sanidine) qui diffèrent de ceux des dykes du groupe II qui présentent une texture ophitique partiellement préservée et des plagioclases moins calciques (albite à labradorite). La variation du Mg# et de l'indice de différenciation (DI) indique que le groupe I (Mg# = 55–65, DI = 16,26–20,19) est plus primitif dans sa composition que le groupe II (Mg# = 30–35, DI = 22,82–50,00). Les valeurs des terres rares et d'autres éléments incompatibles sont plus élevés dans le groupe II que dans le groupe I, et les pentes des spectres de terres rares sont parallèles entre elles, ce qui suggère que les deux groupes sont co-génétiques et que les unités du groupe II sont des magmas plus évolués que ceux du groupe I. La présence des valeurs négatives de Nb et de Ta normalisés par rapport au manteau primitif dans les deux groupes et les rapports La_n/Yb_n (4,73–6,21) suggèrent que le magma a été formé par la fusion partielle d'une lherzolite à grenat hydratée du manteau lithosphérique, modifiée par l'interaction avec la lithosphère précédemment métasomatisée dans le contexte de subduction. Les minéraux d'altération tels que la ferro-édénite et la chlorite sur les marges des cristaux d'augite indiquent une altération deutérique ultérieure ou un métamorphisme tardi-magmatique de faible grade. La chimie de l'échantillon SD (Samira Dyke, un échantillon de la fosse de Libiri dans la mine de Samia, a été précédemment daté à 1791 ± 3 Ma et apparient aux dykes du groupe II) suggère que l'ensemble de l'essaim de dykes orientés NNO-SSE à NNE-SSO appartient à l'essaim Libiri d'une grande province ignée générée par le panache qui s'étend jusqu'à la Sarmatie (Baltica) et l'Amazonie, autrefois adjacentes.

Mots-clés : Géochimie / dykes / provinces ignées géantes / essaim / Niger / petrography

1 Introduction

The spatio-temporal extent of mafic magmatism in the West African Craton has been determined from studies of mafic and ultramafic rocks in the Reguibat and Léo-Man shields and in intra-cratonic sedimentary basins. Among the mafic rocks are dyke swarms and dolerite sills, which are most often parts of the distribution systems of Large Igneous Provinces (LIPs) (Bryan and Ferrari, 2013; Ernst and Buchan, 2002; Ernst *et al.*, 2013). The first mafic magmatic events (LIPs) in the West African Craton were recognized in the Archean around 2733 Ma (Tait *et al.*, 2013). Other events are noticed in the basement formations between 2688 Ma and 580 Ma (Hafid *et al.*, 2001; Aifa *et al.*, 2001; Ama Salah, 1991; Baratoux *et al.*, 2019; Cournède, 2010; Ernst *et al.*, 2021; Kouyaté *et al.*, 2013; Lefort and Aifa, 2001; Potrel *et al.*, 1998; Söderlund *et al.*, 2013a; Tait *et al.*, 2013; Tapsoba *et al.*, 2018; Thomas *et al.*, 2002; Walsh *et al.*, 2002; Youbi *et al.*, 2013; Youbi *et al.*, 2020) and reached a paroxysm in sedimentary basins at 200 Ma with the Central Atlantic LIP (Baratoux *et al.*, 2019; Bassot *et al.*, 1986; Chabou *et al.*, 2007; Chabou *et al.*, 2010; Rooney *et al.*, 2010; Verati *et al.*, 2005). Research on global reconstructions (*e.g.*, Baratoux *et al.*, 2019; Jessell *et al.*, 2015; Youbi *et al.*, 2011) has demonstrated that the mafic dykes with ages between *ca.* 580 Ma and c. 200 Ma belong to three LIPs: 580-550 Ma CIMP – Central Iapetus Magmatic Province (Thomas *et al.*, 2002; Youbi *et al.*, 2020), 369–250 Ma EUNWA: European North West African Magmatic Province (Moutbir *et al.*, 2024; Youbi *et al.*, 2011) and 201 Ma CAMP: Central Atlantic Magmatic Province (Marzoli *et al.*, 2018), while those with ages between c. 2733 Ma and 580 Ma are currently associated with other LIPs. In the Paleoproterozoic domains of the West African Craton, which represents the host rock of younger LIPs, in addition to this radiometric evidence, geochemical studies have indicated the existence of ca. 2040–2060 Ma tholeiitic magmatism potentially also representing a LIP occurring during the Eburnean orogeny (Ama Salah *et al.*, 1996; Augustin and Gaboury, 2017; Baratoux *et al.*, 2011; Béziat *et al.*, 2000; Dampare *et al.*, 2008; Kouyaté *et al.*, 2013; Pawlig *et al.*, 2006; Sakyi *et al.*, 2020; Senyah *et al.*, 2016; Soumaila *et al.*, 2004; Vidal *et al.*, 1996).

In the Liptako area in Niger, tholeiitic magmatism was studied in Paleoproterozoic metabasalts and metagabbros (Ama Salah, 1991; Ama Salah *et al.*, 1996; Affaton *et al.*, 2000; Garba Saley, 2022; Hallarou, 2021; Soumaila, 2000; Soumaila *et al.*, 2004, 2008, 2016a, 2016b) and post Birimian doleritic dykes (Ama Salah, 1991; Baratoux *et al.*, 2019; Machens, 1973; Noura *et al.*, 2023a). Petrographical, geochemical and geochronological data from the literature on the Liptako area dolerites concerned dykes with trends N010°-N020°, N110°-N120° and N130°-N140°. Radiometric dating on the N010°-N020° swarm provided a robust U-Pb baddeleyite age of 1791 ± 3 Ma on a N010° dyke (Baratoux *et al.*, 2019), and an K/Ar biotite age of c. 1010–1370 Ma on a N020° dykes (Ama Salah, 1991). For the N130°–N140° swarm a K/Ar on biotite age of *ca.* 896 Ma, was obtained for a N135° dyke (Ama Salah, 1991). Geochemistry study conducted on the N020°, N110°–N120° and N130°–N140° trending dykes indicate continental tholeiitic and enriched mid-ocean ridge basalts characteristics (Ama Salah, 1991; Noura *et al.*, 2023a) However, the Liptako doleritic dykes are represented by other trends varying between NNE (N000°–N015°) and NNW (N170°) highlighted in areas that have not been studied to date. The N010° trending Libiri dyke (which belongs to the NNE trend) was previously dated at 1791 ± 3 Ma by U-Pb on baddeleyite (Baratoux *et al.*, 2019) on a sample from the Libiri gold mine pit.

The aim of this publication is to provide new information on the genesis and magmatic evolution of the NNW-NNE trending Libiri doleritic dyke swarm of Niger Liptako through a mineralogical and geochemical study, to assess their geodynamic setting.

2 Geological setting and sampling

The West African Craton, stabilized at the end of the Paleoproterozoic (c. 1.9 Ga), forms a vast complex of Archean (c. 3.6–2.6 Ga) and Paleoproterozoic (c. 2.3–2.0 Ga) rocks that form the present-day configuration of the Léo-Man and Reguibat shields (Baratoux *et al.*, 2011; Béziat *et al.*, 2000; Egal *et al.*, 2002; Gasquet *et al.*, 2003; Hirdes and Davis, 2002; Koffi *et al.*, 2022; Kouamelan *et al.*, 2018; Liégeois *et al.*, 1991; Lompo, 2009; Naba, 2007; Parra-Avila, 2017; Sakyi *et al.*, 2020; Senyah *et al.*, 2016; Thiéblemont *et al.*, 2004; Vegas *et al.*, 2008). These two shields are separated by the Taoudeni sedimentary basin. The Precambrian domains and their younger sedimentary cover were injected by mafic intrusions, notably doleritic dykes and sills, whose spatial distribution and grouping into discrete swarms based on trend was interpreted from the regional aeromagnetic map (Baratoux *et al.*, 2019; Jessell *et al.*, 2015) (Fig. 1). This map in Jessell *et al.* (2015) contains more than 3,000 dykes classified into 26 distinct orientation swarm types and emplaced during around 10 mafic magmatic events between c. 2733 Ma and c. 200 Ma (Baratoux *et al.*, 2019; Jessell *et al.*, 2015; Noura *et al.*, 2023a).

The Liptako Paleoproterozoic basement is part of the Boulé Mossi domain of the Léo-Man shield. It is located at the NE margin of this domain and consists of two main types of units, greenstone belts and granitoid plutons. Infracambrian and Continental terminal 3 (Oligocene) sedimentary formations mark a major unconformity on the basement (Fig. 2). These greenstone belts and the granitoid plutons follow an overall NE-SW orientation due to Eburnean deformation, and are labelled from south-east to north-west, the Makalondi belt, Torodi pluton, Sirba belt, Dargol-Gothèye pluton, Diagorou-Darbani belt, Tera-Ayorou pluton and Gorouol belt. The greenstone belts consist of metabasites (metabasalts, metadolerites and metagabbros), meta-volcano-clastites (metavolcanic breccia and metatuff) and metasediments (schists, metaconglomerates, metagreywackes) (Ama Salah *et al.*, 1996; Attourabi *et al.*, 2024b; Dupuis *et al.*, 1991; Garba Saley *et al.*, 2024; Hallarou *et al.*, 2020b; Ahmed *et al.*, 2022; Machens, 1973; Noura *et al.*, 2023a; Soumaila *et al.*, 2008; Soumaila *et al.*, 2016a,b). The emplacement ages of the greenstone belts have been determined from micaschists and metabasalts and range from 2400 ± 42 Ma to 2050 ± 12 Ma (Soumaila *et al.*, 2008). The granitic massifs consist of tonalities, trondhjemites, and granodiorite series rocks intruded by plutonic bodies of various suites of granites, diorites and syenites (Abdou *et al.*, 1998; Ahmed *et al.*, 2022; Ama Salah *et al.*, 1996; Attourabi *et al.*, 2024b; Cheilletz *et al.*, 1994; Dupuis *et al.*, 1991; Lama, 1993; Pons *et al.*, 1995; Soumaila, 2000). U/Pb, Sm-Nd and K/Ar ages obtained from Liptako granitoids range from 2000 ± 60 Ma to 2188 ± 12 Ma (Abdou *et al.*, 1998; Ama Salah *et al.*, 1996; Cheilletz *et al.*, 1994; Dupuis *et al.*, 1991; Lama, 1993; Pons *et al.*, 1995; Soumaila *et al.*, 2008). These greenstone belts and granitoids plutons are crosscut by quartzite, quartzo-feldspathic and pegmatitic veins (Ahmed *et al.*, 2022; Attourabi *et al.*, 2024b; Pons *et al.*, 1995; Soumaila, 2000). On the geological map of Machens (1973) (Fig. 2), doleritic dyke trend in four major orientations: NNW-NNE, NW-SE, WNW-ESE, E-W. The NNW-NNE swarm, which is the subject of this publication, is characterized by a range in trends between NNE (N000°–N015°) and NNW (N170°). The dykes of this swarm are observed in outcrop in greenstone belt rocks and in granitoid plutons, in the form of irregular lines of blocks covered with a brownish alteration patina (Figs. 3a and 3b). The doleritic dykes were sampled in the areas of the Tera-Ayorou and Dargol-Gotheye plutons and the Diagorou-Darbani and Sirba greenstone belts (Fig. 2). The specific trends measured at the sampling localities and dyke thicknesses are listed in Table 1. We collected at least 2 samples from each dyke of N000°–N015° and N170° trends. The SD sample in Table 1 was collected in the Libiri gold mine and corresponds to the N010° Libiri swarm dated with a precise U-Pb age of 1791 ± 3 Ma (Baratoux *et al.*, 2019). N020° and N140° trending dykes given less precise ages obtained by the K-Ar method ranging from 1378 ± 36 Ma to 1011 ± 46 Ma and 896 ± 25 Ma (Ama Salah, 1991), respectively.

3 Methodology

3.1 Thin section chemical mapping and electron microprobe analyses

Thin section chemical mapping and electron microprobe analyses were done at the GET Laboratory and Raimond Castaing Microanalytical Center of the University of Toulouse (France), respectively. One thin section was prepared from each collected sample. The instrument used for mapping and electron microprobe analyses was a Tescan Vega 4 LMU SEM (partial vacuum), coupled with Bruker Quantax SDD-type EDX 30 mm^2 detector. The current used was 15 kV, the working distance varied from 10 to 16 mm, the pixel size was between 50 and 70 μm and magnification between 5 and 1000. The chemical mapping was used to characterize the zonations and spatial distribution of Ca, Mg, Al, Fe, Si, Ti, Na and K in pyroxene, Fe-Ti oxides, amphibole and feldspar crystals. Mineral chemistry was determined using the CAMECA SXFive electron microprobe (EPMA). The beam had 2 μm and was characterized by a voltage of 15 kV and a current of 10 nA. Standard minerals analyzed included albite (Na), baryte (Ba), Cr_2O_3 (Cr), corundum (Al), hematite (Fe), periclase (Mg), wollastonite (Si, Ca), sanidine (K), $MnTiO_3$ (Ti, Mn), topaz (F), silicon aluminate glass with RB_2O and Cs_2O (Rb, Cs), and graftonite (P). Chemical maps and microprobe analyses on feldspars, pyroxene, amphibole and biotite were carried out on the SD, SLB, TD1 and TD2 samples and over twenty selected points were analyzed from each mineral to average out any chemical variability.

3.2 Geochemical analyses

Fifteen samples were analyzed at the ALS Geochemistry laboratory (Canada) by using ICP-MS (Inductively Coupled Plasma-Mass Spectrometry) coupled with ICP-AES (Atomic Emission Spectrometry) for whole rock major oxides and trace elements.

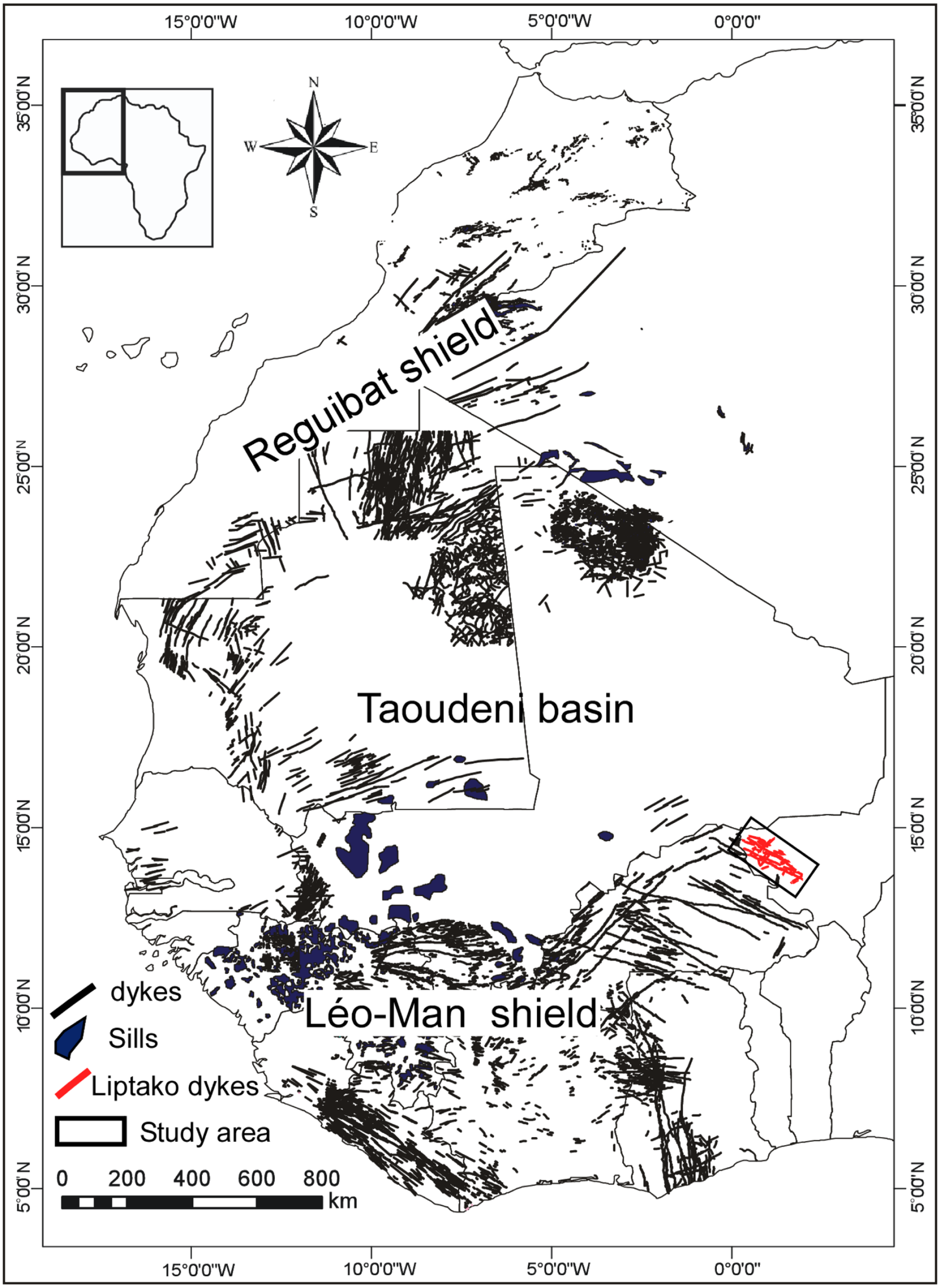

Fig. 1. Map of mafic sills and dykes in the West African Craton (Jessell *et al.*, 2015), with modifications in red based on mapping from aeromagnetic overflights of the Liptako area dykes (ACDI, 1973).

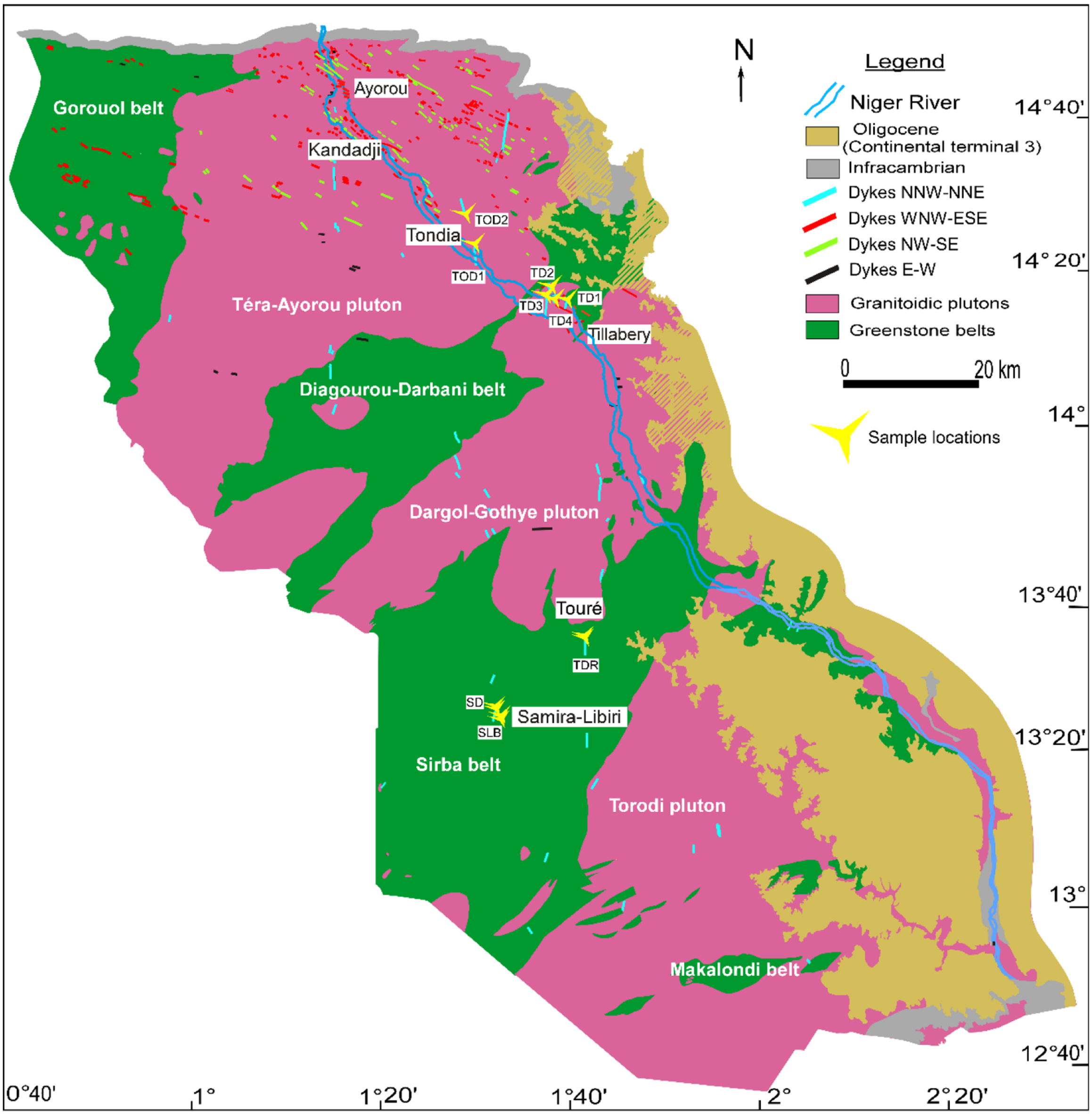

Fig. 2. Geological map of the Liptako area in Niger (Machens, 1973). The different trends are color coded and refer to different swarms. The dated N010° Libiri swarm at 1791 Ma (Baratoux *et al.*, 2019) belong to Samira-Libiri sector.

4 Results

4.1 Petrography

The doleritic textures, mineralogical compositions and degree of mineral alterations of the Libiri NNW-NNE dykes reveal two main petrographic types. The first type is characterized by dolerites with a well-preserved intergranular texture and the constituent minerals are plagioclase, K-feldspar, clinopyroxene, orthopyroxene, apatite, amphibole, biotite, sericite, chlorite, Fe-Ti oxides, and K-feldspar intergrowns with quartz showing the granophyric texture (Figs. 3c and 3d). This petrographic type comprises the SD, SLB and TDR dykes with N000° and N010° trends, intrusive into the Sirba greenstone belt. The second type consists of dolerites with a partially preserved ophitic texture. In this type, the same minerals are found as in the first one, with the exception of orthopyroxene, which is absent in the second type, while it contains epidote (Figs. 3e and 3f).This type is found in the TOD and TD dykes with N000° to N170° trends, cross-cutting the Tera-Ayorou and Dargol-Gotheye plutons and in the Diagorou-Darbani greenstone belt. Based on the bulk rock geochemical analyses (Sect. 4.3), the dykes were divided into two chemical groups (Tab. 1), which partially correspond to the petrographic types. In this case, the sample TD1 belongs petrographically to the first type but chemically to the second group. We will use these two geochemical groups when describing the chemical maps (Sect. 4.2), electron microprobe analysis results (Sect. 4.2) and geochemical composition of whole-rock (Sect. 4.3).

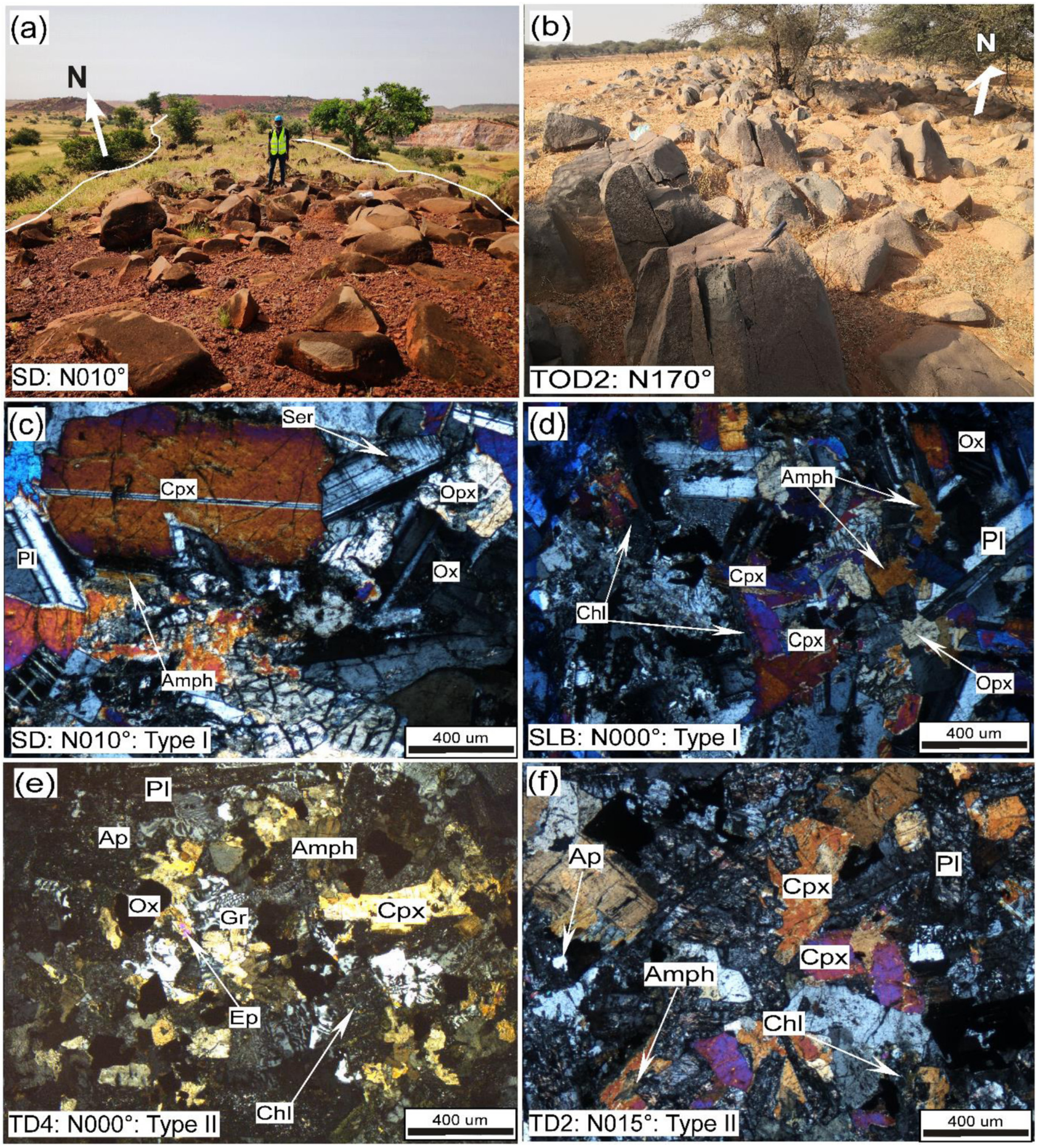

Fig. 3. Field and petrographic photos of the NNW-NNE Libiri swarm: (a and b) outcrop mode of doleritic dykes from this swarm and (c, d, e and f) microphotographs showing typical textures and representative minerals in both petrographic types. Pl: plagioclase, Opx: orthopyroxene, Cpx: clinopyroxene, Amph: amphibole, Chl: chlorite, Ap: apatite, Ox: Fe-Ti oxides, Ep: epidote.

Table 1. Characteristics of sampled dykes of the NNW-NNE Libiri swarm.

Groups of the NNW-NNE Libiri swarm	Symbol dykes	Dyke orientations	Dyke thicknesses
Group I	SD : Samira dyke	N010°	60 m
	SLB : Samira Libdorado	N000°	45 m
	TOD1 : Tondia Dyke 1	N170°	50 m
	TOD2 : Tondia Dyke 2	N000°	60 m
	TD1 : Tillabéri Dyke 1	N015°	7 m
	TDR : Touré Dyke	N000°	30 m
Group II	TD2 : Tillabéri Dyke 2	N015°	5 m
	TD3 : Tillabéri Dyke 3	N010°	10 m
	TD4 : Tillabéri Dyke 4	N000°	15 m

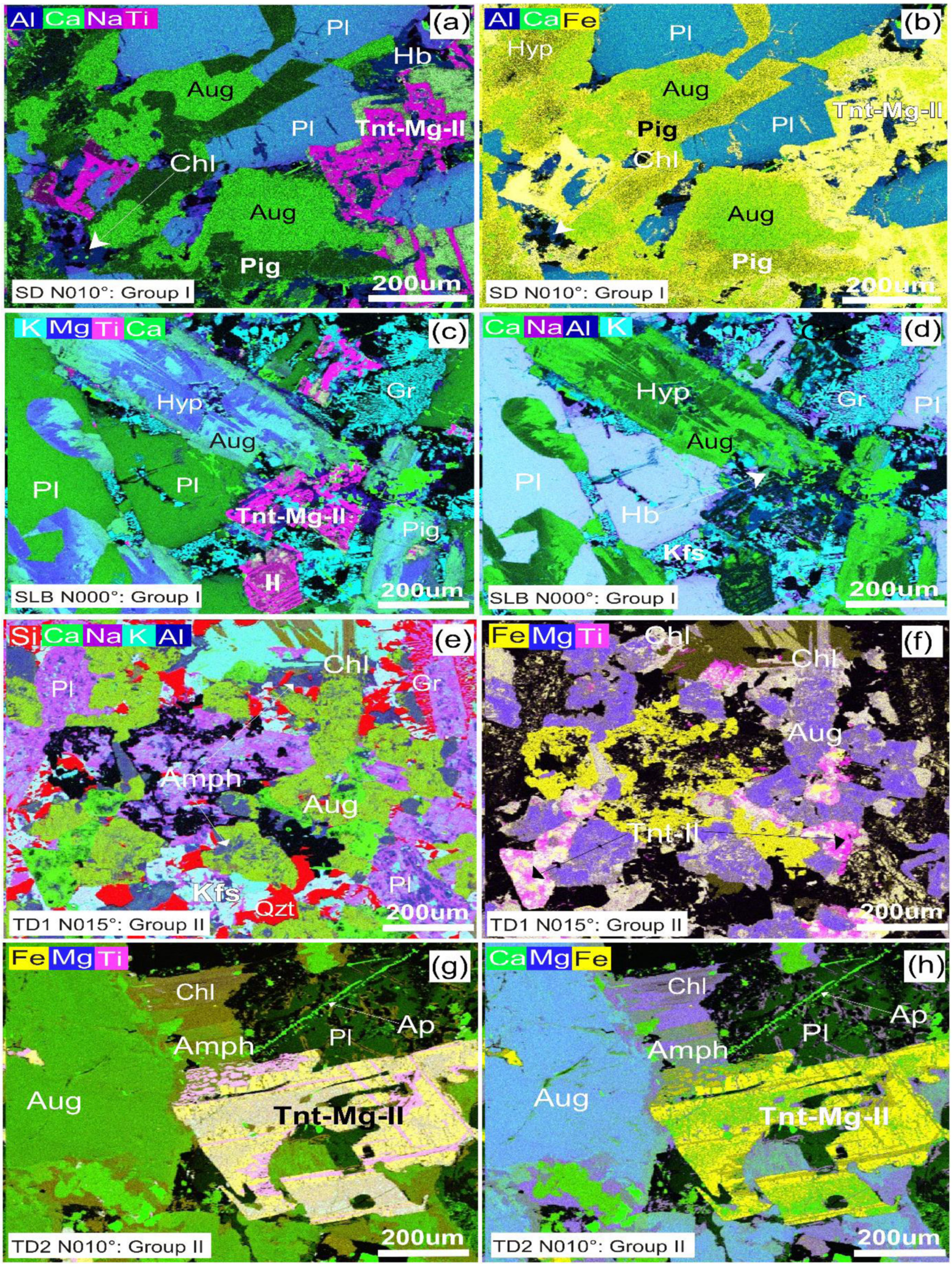

Fig. 4. Chemical maps of SD, SLB, TD1 and TD2 dykes belonging to both groups. Pl: plagioclase, Aug: augite, Pig: pigeonite, Hyp: hypersthene, Amph: amphibole, Kfs: K-feldspars, Ap: apatite, Gr: grain with granophyric texture, Tnt-Mg-Il: titanomagnetite-ilmenite.

4.2 Mineralogy

4.2.1 Feldspars

Feldspars are represented in both geochemical groups by plagioclase which occurs in Group I dykes as divergent laths showing albite-type polysynthetic twins (Figs. 3c and 3d) while it correspond to the relict laths in Group II dykes. The laths are affected by sectorial sericite development in Group I dykes and more albitized in Group II dykes. The proportion of plagioclase crystals varies depending on the texture of the

Table 2. Selected points are representative electron microprobe analysis results of feldspars.

Sample	TD2	TD1	TD1	TD2	SD	SD	SLB	SD
Minerals	Albite	Oligoclase	Andesine	Labradorite	Labradorite	Bytownite	Sanidine	Anorthoclase
SiO_2	64.300	60.250	56.040	53.940	51.820	49.030	72.130	70.960
TiO_2	0.000	0.010	0.000	0.090	0.020	0.000	0.050	0.030
Cr_2O_3	0.000	0.010	0.000	0.010	0.000	0.000	0.000	0.000
Al_2O_3	22.000	24.410	26.120	28.140	28.570	30.730	14.440	15.700
Fe_2O_3	0.000	0.000	0.000	0.142	1.300	0.733	0.000	0.000
FeO	0.660	0.410	0.750	0.742	0.000	0.000	0.070	0.110
MnO	0.020	0.040	0.000	0.000	0.000	0.070	0.000	0.000
NiO	0.010	0.000	0.010	0.020	0.030	0.050	0.000	0.010
MgO	0.210	0.010	0.040	0.110	0.170	0.340	0.000	0.010
CaO	1.660	6.380	9.360	11.630	13.030	15.340	0.130	0.150
Na_2O	8.850	7.400	5.700	4.740	3.980	2.840	1.220	2.780
K_2O	1.850	0.390	0.380	0.150	0.330	0.280	11.330	11.230
Total	99.560	99.310	98.400	99.714	99.250	99.413	99.370	100.98
Numbers of ions based on 8 oxygens								
Si	2.860	2.711	2.569	2.453	2.380	2.255	3.396	3.206
Ti	0.000	0.000	0.000	0.003	0.001	0.000	0.002	0.001
Cr	0.000	0.000	0.000	0.000	0.000	0.000	0.000	0.000
Al	1.153	1.295	1.411	1.509	1.547	1.666	0.801	0.889
Fe3+	0.000	0.000	0.000	0.005	0.045	0.025	0.000	0.000
Fe2+	0.025	0.015	0.029	0.028	0.000	0.000	0.003	0.004
Mn	0.001	0.002	0.000	0.000	0.000	0.003	0.000	0.000
Ni	0.000	0.000	0.000	0.001	0.001	0.002	0.000	0.000
Mg	0.014	0.001	0.003	0.007	0.012	0.023	0.000	0.001
Ca	0.079	0.308	0.460	0.567	0.641	0.756	0.007	0.007
Na	0.763	0.646	0.506	0.418	0.354	0.253	0.111	0.244
K	0.105	0.022	0.022	0.009	0.019	0.016	0.680	0.647
Total	5.000	5.000	5.000	5.000	5.000	5.000	5.000	5.000
Ca [An]	0.084	0.315	0.465	0.570	0.632	0.737	0.008	0.008
Na [Ab]	0.806	0.662	0.512	0.421	0.349	0.247	0.139	0.271
K [Or]	0.111	0.023	0.022	0.009	0.019	0.016	0.852	0.721

dykes. It is estimated in Group II dykes at around 40–45% whereas it accounts around 50–60% in Group I dykes. The altered crystals are transparent in natural polarized light or show a gray-black haze due to sericite alteration (Figs. 3c and 3d) and are surrounded by transparent apatite and/or brownish clinopyroxene crystals (Figs. 3e and 3f).

Chemical maps show variable chemical distributions of Ca, Na and K between the cores and margins of feldspar crystals (Fig. 4). In dykes belonging to Group I, plagioclase is characterized by a high concentration and homogeneous distribution of Ca between the cores and margins of the laths, whereas in dykes belonging to Group II, the laths are less Ca-rich and show a heterogeneous distribution of Na. Na-rich laths are often associated with K-rich or Si-rich grains and correspond to alkali feldspars (Kfs) or quartz and K-feldspar grains with granophyric texture (Gr), respectively (Figs. 4b, 4c, and 4e).

The electron microprobe analyses results of feldspars of both groups are shown in Table 2. Projection of these results in the Ab – Or – An diagram (Fig. 5a), shows a continuum of compositions from Ab_{25} to Ab_{96}. Group I dykes are characterized by rare K-feldspars (orthoclase and sanidine) and calcic plagioclase with labradorite ($Ab_{40–43}$-$An_{55–58}$) and bytownite ($Ab_{25–29}$-$An_{70–74}$). Group II dykes contain less calcic plagioclase, ranging from albite (Ab_{96}-An_4), to labradorite ($Ab_{42–48}$-$An_{51–57}$). These An# values indicate that the Group I dykes are more primitive than Group II dykes. The presence of less calcic plagioclase in Group II dykes can be explained by fractional crystallization or albitization of early formed plagioclase crystals during deuteric alteration in a magma chamber.

4.2.2 Pyroxene, amphibole, chlorite

Pyroxene is represented by orthopyroxene and clinopyroxene in Group I (Figs. 3c and 3d), while in Group II, only clinopyroxene was found (Figs. 3e and 3f). In both groups, large clinopyroxene crystals locally show growth twins, which are overgrown by brown amphibole (Tab. 3, Figs. 3c, 3d, 3e, and 3f, Fig. 5c) or greenish-gray chlorite fibers (Figs. 3c, 3d, 3e, and 3f). Some large amphibole crystals are locally transformed into epidote in Group II dykes (Fig. 3e). These characteristics indicate a pseudomorphosis

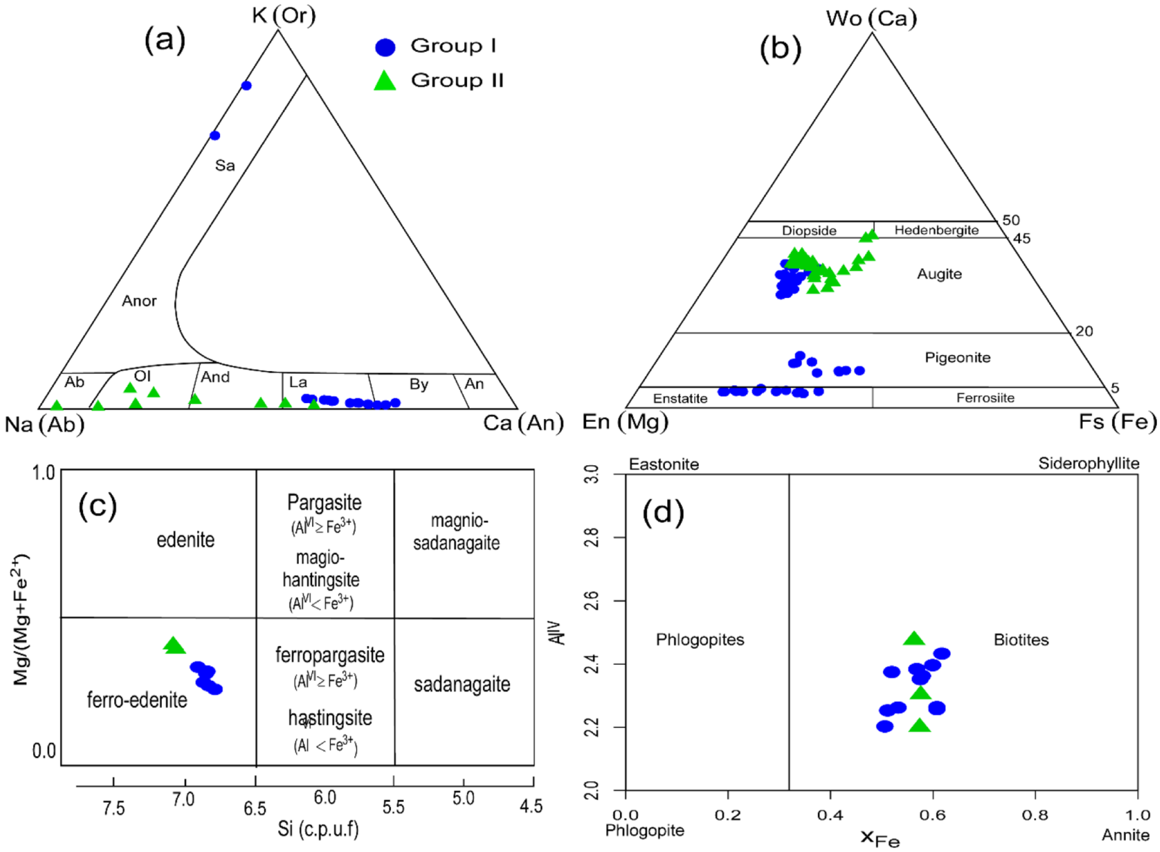

Fig. 5. Compositional diagrams of (a) feldspar, (b) pyroxene (Morimoto *et al.*, 1988), (c) amphibole (Leake *et al.*, 1997) and (d) biotite (Speer, 1984 and Deer *et al.*, 1986) of boths groups. Ab: albite, Ol: oligoclase, And: andesine, La: labradorite, By: bytownite, An: anorthite. Symbols with blue circles belonging to Group I and green triangles belonging to Group II.

after uralitization of clinopyroxene crystals during interaction with late magmatic fluids or deuteric alteration.

The distribution of chemical elements within pyroxene crystals in the chemical maps (Figs. 4 and 5) shows zonation between Ca, Mg and Fe corresponding to augite, pigeonite and hypersthene compositions in Group I dykes whereas it indicates augite compositions in Group II dykes. Representative electron microprobe analysis results of selected points of pyroxenes in both groups are provided in Table 4. In the Wo – En – Fs diagram (Morimoto *et al.*, 1988, Fig. 5a), the chemical compositions of pyroxenes in dykes belonging to Group I vary between those of augites ($Wo_{30–38}$-$En_{42–53}$-$Fs_{13–20}$), pigeonites ($Wo_{5–14}$-$En_{46–67}$-$Fs_{25–43}$) and clinoenstatite ($Wo_{4–5}$-$En_{59–78}$-$Fs_{18–37}$). On the other hand, for dykes belonging to Group II, compositions fall between the augite range ($Wo_{31–41}$-$En_{33–47}$-$Fs_{14–29}$) and those of diopside ($Wo_{45–46}$-$En_{27–29}$-$Fs_{26–27}$). Pyroxenes in dykes belonging to Group I are relatively richer in Cr_2O_3 (0.11–0.67 wt%) and poorer in TiO_2 (0.11–0.67 wt%) than those in dykes belonging to Group II (Cr_2O_3 = 0.00–0.24 wt%, TiO_2 = 0.18–0.83 wt%). As indicated in Table 4, pyroxenes in both groups are characterized by an Al^{IV}/Al^{VI} ratio >1, typical of pyroxenes of mantle melt origin (Marcelot *et al.*, 1983; Porras, 2010). In Group I, significant chemical zonation is observed in chemical maps within augite crystals, with Fe-Ca-rich cores and slightly Ca-poor margins, while within pigeonite and hypersthene crystals, Mg-rich cores and Mg-poor margins are observed (Figs. 4 and 5). In Group II dykes, augites are characterized by Ca-rich crystal interiors and Fe-Mg-Al-rich crystal margins, which correspond to amphibole or chlorite. Projection of the analytical results for amphibole (Tab. 3) for both groups into the Leake *et al.* (1997) classification diagram, shows that it corresponds to ferro-edenite (Fig. 6c).

4.2.3 Biotite

Biotite is identified on the microphotographs and chemical maps as crystals size below to 70 µm. Microprobe results (Tab. 5) show that it contains traces of MnO (0.01–0.25 wt%) and Na_2O (0–0.32 wt%) and relatively high content of TiO_2 (0.05–4.71 wt%). In the mica classification diagram of Speer (1984) and Deer *et al.* (1986), the small grains plot within the biotite field with X_{Fe} = 0.5–0.65 and Al^{IV} = 2.1–2.5 (Fig. 5d).

4.2.4 Apatite

Apatite is found as grains size below to 60 µm in plagioclase laths. On the chemical maps, it is mainly distinguished as Ca-rich grains or filaments in both groups (Fig. 4g).

Table 3. Selected points are representative electron microprobe analysis results of amphibole. Numbers of ions is based on 23 oxygens.

Samples	TD2	SLB	SD
Mineral	Fe-edenite	Fe-edenite	Fe-edenite
Na_2O	1.72	1.62	1.71
MgO	8.41	5.67	6.69
Al_2O_3	5.42	6.53	6.46
SiO_2	46.11	43.92	43.63
Cl^-	0.33	0.35	0.31
K_2O	0.58	0.80	0.69
CaO	9.76	10.19	9.94
TiO_2	1.24	1.54	1.39
Cr_2O_3	0.00	0.02	0.03
MnO	0.270	0.260	0.330
FeO	23.14	27.24	25.47
NiO	0.05	0.05	0.00
Total	97.03	98.21	96.66
Al^{IV}	0.85	1.092	1.085
Si	7.15	6.908	6.915
Mg	1.944	1.330	1.581
Al^{VI}	0.141	0.119	0.122
Ti	0.145	0.182	0.166
Cr	0.000	0.002	0.004
Na	0.517	0.494	0.525
Fe^{2+}	3.001	3.583	3.376
K	0.115	0.161	0.140
Ba	0.000	0.001	0.001
Cl	0.087	0.093	0.083
OH	1.913	1.907	1.917
Total	15.862	15.872	15.914
Ca_B	1.622	1.717	1.688
Si (c.p.u.f.)	7.15	6.908	6.915
$(Na+K)_A$	0.526	0.63	0.646
Ti	0.145	0.182	0.166

4.2.5 Fe-Ti oxides

Fe-Ti oxides occur as subautomorphic or xenomorphic crystals in the coarse-grained portions of dykes, isolated or arranged around amphibole and chlorite crystals (Figs. 3c, 3d, 3e, and 3f). In some finer grained portions, Fe-Ti oxides are located in the interstices between plagioclase laths. On chemical maps, we distinguish subautomorphic crystals which are rich in Fe, Ti and Ca; corresponding to titano-magnetite-ilmenite (Fig. 4).

4.3 Geochemistry

4.3.1 Major and trace elements

Whole-rock analyses of major (wt%) and trace (ppm) elements of both groups are listed in Tables 6 and 7. The two petrological groups described above show significant bulk rock composition differences. Exceptions are the SiO_2 contents which range from 51.0 to 54.2 wt% for Group I dykes and 54.7 to 56.6 wt% for Group II dykes. Na_2O+K_2O contents are low in Group I (2.65–2.82 wt%) and relatively high in Group II (3.61–4.52 wt%). Group I dykes have TiO_2 and Fe_2O_3 contents relatively low ($TiO_2 = 0.74–0.89$ wt%, $Fe_2O_3 = 11.15–11.9$ wt%) compared to Group II dykes ($TiO_2 = 1.34–1.38$ wt%, $Fe_2O_3 = 13.60–15.35$ wt%). However, MgO and CaO contents are high in Group I (MgO = 7.41–8.54 wt%, CaO = 8.73–9.42 wt%) and low in low in Group II (MgO = 2.90–3.47 wt%, CaO = 6.03–6.81 wt%). The difference in SiO_2 and Na_2O+K_2O contents presented by both groups is probably due to deuteric or hydrothermal alteration. For example, the effects of hydrothermal alteration are visible on microphotographs (Fig. 3) and chemical maps of Group II dykes (Figs. 4e, 4f, 4g, and 4h) and are exhibited by the destabilization of augite and plagioclase crystals. The low variation in MgO, TiO_2 and CaO contents between the two groups can be associated with the magma evolution during high-Ca plagioclase and hypersthene-pigeonite-augite fractionation (Figs. 5a and 5b, Fig. 7b).

Mg# (100*((MgO/40.32)/(MgO/40.32+FeO(FeO = 0,9889*Fe_2O_3)/71.85)), (Grill, 2010) varies from 56 to 65 in Group I dykes and 30 to 35 in Group II dykes. This is indicated by the Mg# parameter in Figure 6 as two distinct geochemical groups. In total-alkali silica (TAS) diagram (Le Bas *et al.*, 1986), (Fig. 8a), samples show two clusters of basaltic andesite to andesite composition with an evolved tholeiitic character. However, in Al-Fe^T+Ti-Mg (Fig. 8b), Group I dykes show characteristics similar to tholeiite basalt with high magnesium contents whereas Group II dykes have affinity close to tholeiite basalt with high iron contents.

Group I dykes show high Cr contents (344–505 ppm), while Group II dykes have lower contents (34–66 ppm). Zr and Nb contents are low in Group I (Zr: 88–116 ppm, Nb: 3.77–6.00 ppm) and relatively high in Group II (Zr: 152–175 ppm and Nb: 6.37–7.58 ppm). Ta and Yb contents are low in Group I (0.1–0.2 ppm and 1.65–2.26 ppm) and high in Group II (Ta: 0.4–0.5 ppm, Yb: 2.40–2.87 ppm

Extended primitive mantle normalized trace-elements, marked “N”, (Sun & McDonough, 1989) and chondrite normalized, marked as “n”, Boynton, 1983 plots for both groups (Fig. 7) are characterized by moderately sloping profiles. The mantle-normalized plot (Fig. 7a) displays positive peaks in Ba, U, Nd and K and negative peaks in Nb, Ta, P, and Ti. The Th_N/La_N (1.00–1.29) and Th_N/Nb_N (2.96–4.13) ratios are low in Group I and relatively higher in Group II (Th_N/La_N: 1.31–1.42; Th_N/Nb_N: 4.18–4.53). The chondrite-normalized REE plot (Fig. 7b) is characterized by LREE enrichment and a low La_n/Yb_n (4.73–5.51) ratio for the dykes belonging to Group I and a higher one for the dykes belonging to Group II ($La_n/Yb_n = 5.14–6.21$). The Ce_n/Yb_n (3.49–4.60) ratio is higher in Group II than in Group I ($Ce_n/Yb_n = 2.21–2.44$). All samples show negative Eu anomalies, with values decreasing slightly from Group I (Eu/Eu* = 0.79–0.93) to Group II (0.78–0.84), suggesting plagioclase fractionation.

5 Discussion

5.1 Hydrothermal and deuteric alterations

As demonstrated above, the NNW-NNE Libiri swarm can be divided into two petrological types based on their textures

Table 4. Selected points are representative electron microprobe analysis results of pyroxene.

Samples	SD	SD	SD	TD1	TD1	SLB	TD2
Mineral	Augite	Pigeonite	Hypersthene	Augite	Diopside	Pigeonite	Augite
SiO_2	52.43	51.98	53.88	51.3	49.93	52.92	51.22
Na_2O	0.18	0.06	0.03	0.29	0.57	0.11	0.30
MgO	17.00	20.42	28.12	15.65	9.07	20.49	14.98
Al_2O_3	1.74	1.49	2.72	2.56	1.40	1.48	2.10
K_2O	0.00	0.02	0.00	0.01	0.00	0.00	0.00
CaO	16.51	6.85	2.16	18.67	21.37	7.58	17.79
TiO_2	0.30	0.32	0.15	0.70	0.20	0.28	0.72
Cr_2O_3	0.17	0.20	0.46	0.11	0.02	0.11	0.02
MnO	0.25	0.30	0.16	0.24	0.71	0.39	0.32
FeO	10.87	17.67	11.36	9.5	15.45	16.18	11.25
NiO	0.03	0.03	0.10	0.05	0.00	0.04	0.04
Total	99.48	99.34	99.14	99.08	98.85	99.58	98.74
Numbers of ions based on 6 oxygens							
Al^{IV}	0.04	0.053	0.067	0.078	0.044	0.036	0.063
Si	1.94	1.946	1.932	1.922	1.956	1.963	1.937
Na	0.01	0.004	0.002	0.021	0.043	0.007	0.022
Mg	0.94	1.140	1.503	0.874	0.53	1.133	0.844
Al^{VI}	0.028	0.012	0.047	0.035	0.021	0.028	0.030
K	0.00	0.00	0.000	0.000	0.000	0.000	0.00
Ca	0.65	0.274	0.083	0.75	0.897	0.301	0.720
Ti	0.008	0.009	0.004	0.02	0.006	0.007	0.020
Cr	0.005	0.005	0.013	0.003	0.001	0.003	0.000
Mn^{2+}	0.007	0.009	0.004	0.008	0.024	0.012	0.010
Fe^{2+}	0.338	0.5534	0.3407	0.298	0.506	0.502	0.355
Total	4.004	4.009	3.998	4.009	4.027	3.997	4.0052
Al^{IV}/Al^{VI}	1.652	4.341	1.441	2.228	2.095	1.257	2.058
Wo (Ca)	0.338	0.139	0.043	0.3886	0.4585	0.1546	0.3732
En (Mg)	0.4842	0.5764	0.7782	0.4532	0.2707	0.5815	0.4373
Fs (Fe)	0.1777	0.2846	0.1789	0.1583	0.2708	0.2639	0.1895

and degree of alteration. The two types correspond partially, but not completely, to two groups determined using the bulk rock geochemistry. The mineral chemistry also shows systematic differences between these two groups. The Group I dykes are more primitive and less altered than Group II dykes. The presence of orthopyroxene and more calcic plagioclase in Group I dykes compared to Group II dykes can be associated to the magma evolved during minerals fractionation whereas the difference in dyke textures and altered crystals can be explained by deuteric or hydrothermal alteration. Petrographic characteristics of Group I dykes are similar to the results obtained by Ama Salah (1991) on the N020° oriented dykes intersecting the Sirba belt. This author observed an intergranular texture and minerals such as orthopyroxene, clinopyroxene, plagioclase, amphibole, biotite, sericite and Fe-Ti oxides. Group II dykes have the same characteristics as the petrographic results (large ophitic clinopyroxene and plagioclase, amphibole and minor Fe-Ti oxides) described in Baratoux *et al.* (2019) on the N010° Libiri dated dyke, sampled in the Samira gold mine. However, the petrographic characteristics of both group dykes differ from those of the WNW-ESE to NW-SE-trending Liptako area doleritic dykes (ophitic texture, augite, pigeonite, plagioclase, apatite, abundance of chlorite, biotite, Fe-Ti oxides) highlighted by Noura *et al.* (2023a).

The gray-black opacity of plagioclase laths observed in dykes belonging to Group II and the presence of alteration minerals (sericite, epidote and chlorite) on plagioclase, amphibole, augite and biotite crystals observed in dykes of both groups are comparable to results described by Cournède (2010); Sengupta *et al.* (2014); Noura *et al.* (2023a) and interpreted in the West African Craton in relation to alteration activities or a low grade post-magmatic metamorphic process, such as amphibole epidotization, plagioclase sericitization and biotite chloritization. Moreover, the late magmatic minerals (ferro-edenite and biotite) highlighted as isolated crystals or on the margins of augite large crystals in these dykes, are typical of deuteric alteration, but sericite, epidote and chlorite minerals are originating from hydrothermal alteration or low grade post-magmatic metamorphism.

Deuteric alteration can cause significant mineralogical and geochemical changes during the recrystallization of minerals already formed in the magma chamber (Mottl, 1983; Sengupta *et al.*, 2014). Mineralogical change has been highlighted on the

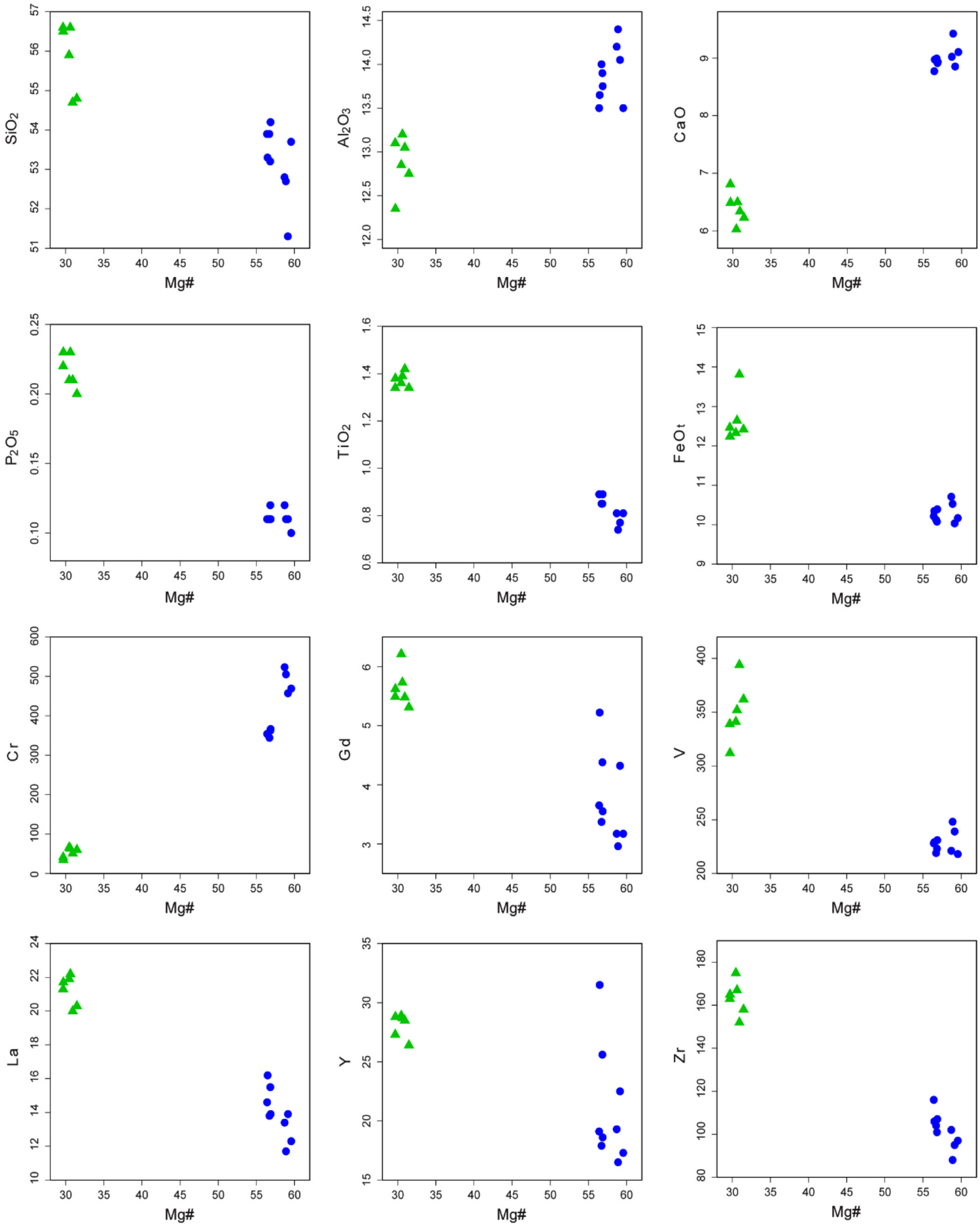

Fig. 6. Diagram of variations in oxides and trace elements as a function of the Mg# parameter. Symbols with blue circles belonging to Group I and green triangles belonging to Group II.

Table 5. Selected points are representative electron microprobe analysis results of biotite. Numbers of ions is based on 22 oxygens.

Samples	SLB	SD	TD2
Mineral	Biotite	Biotite	Biotite
Na_2O	0.00	0.24	0.08
MgO	4.86	10.15	8.47
Al_2O_3	12.26	11.95	11.63
SiO_2	35.94	36.49	37.28
Cl^-	0.01	0.21	0.29
K_2O	6.43	8.01	7.86
CaO	0.00	0.10	0.14
TiO_2	0.05	4.44	3.50
Cr_2O_3	0.01	0.03	0.01
MnO	0.19	0.08	0.11
FeO	33.53	22.8	24.2
NiO	0.00	0.07	0.01
Total	93.28	94.73	93.58
Al^{IV}	2.063	2.203	2.083
Si	5.936	5.707	5.917
Al^{VI}	0.323	0.00	0.093
Mg	1.196	2.367	2.004
Ti	0.006	0.522	0.418
V^{3+}	0.00	0.00	0.00
Cr	0.001	0.004	0.001
Mn^{2+}	0.027	0.011	0.015
Fe^{2+}	4.632	2.982	3.212
Ni	0.00	0.009	0.001
Na	0.00	0.073	0.025
K	1.355	1.598	1.592
Cl^-	0.004	0.004	0.007
OH	3.997	3.944	3.922
Total	19.541	19.424	19.29
X_{Fe}	0.748	0.506	0.559

Table 6. Whole-rock major (wt%) and trace elements (ppm) compositions of Group I dykes. LOI = Loss On Ignition, N = primitive mantle, n = chondrite.

Samples	SD1	SLB1	TDR1	SD1a	SLB1a	TDR1a	TOD1	TOD2	TD1
Lat. N	13.407	13.339	13.567	13.407	13.339	13.567	14.389	14.451	14.264
Long. E	1.254	1.255	1.462	1.254	1.255	1.462	1.211	1.187	1.411
Major elements (wt%)									
SiO_2	52.7	51.3	53.2	52.8	53.7	53.3	53.9	54.2	53.9
Al_2O_3	14.4	14.05	13.90	14.2	13.50	13.65	14.00	13.75	13.50
Fe_2O_3	11.7	11.15	11.2	11.9	11.30	11.50	11.25	11.55	11.35
CaO	9.42	8.85	9.02	9.1	8.91	8.97	8.77	8.93	8.73
MgO	8.46	8.15	7.44	8.54	8.40	7.53	7.44	7.69	7.41
Na_2O	1.88	1.84	1.93	1.89	1.88	1.93	2.13	2.12	2.11
K2O	0.77	0.94	0.79	0.82	0.78	0.80	0.91	0.88	0.86
Cr_2O_3	0.07	0.06	0.05	0.07	0.07	0.05	0.05	0.050	0.048
TiO_2	0.74	0.77	0.85	0.81	0.81	0.89	0.85	0.89	0.89
MnO	0.17	0.16	0.15	0.18	0.16	0.15	0.16	0.16	0.15
P_2O_5	0.11	0.11	0.12	0.12	0.10	0.11	0.11	0.11	0.11
SrO	0.02	0.02	0.02	0.02	0.02	0.02	0.02	0.02	0.02
BaO	0.03	0.05	0.08	0.03	0.03	0.08	0.04	0.03	0.03

Table 6. (continued).

Samples	SD1	SLB1	TDR1	SD1a	SLB1a	TDR1a	TOD1	TOD2	TD1
LOI	0.75	0.86	0.68	0.89	0.60	0.67	1.33	1.06	1.15
Total	101.22	98.31	99.43	101.37	100.26	99.65	100.96	101.44	100.26
Mg#	61.91	62.17	59.89	61.74	62.56	59.55	59.79	59.95	59.48
DI	16.26	17.98	33.55	17.08	18.68	19.37	35.50	19.77	20.19
Trace elements (ppm)									
Ba	264	474	751	281	246	713	327	290	272
Ce	24.2	27.2	31.8	26.8	27.1	30.5	30.0	30.8	32.2
Cr	505	457	362	523	469	354	344	366	354
Cs	0.83	0.77	0.81	1.09	1.00	0.78	0.69	0.67	0.63
Dy	2.88	3.85	3.60	3.53	2.88	4.57	3.16	3.30	3.48
Er	1.76	2.31	2.18	1.64	1.79	2.59	1.83	1.89	1.88
Eu	0.84	1.17	1.20	0.88	0.97	1.28	1.00	1.06	1.03
Ga	17.4	17.4	16.0	16.9	14.4	16.1	16.3	16.5	16.0
Gd	2.96	4.32	4.38	3.17	3.17	5.22	3.37	3.55	3.65
Hf	2.48	2.65	2.71	2.88	2.45	2.62	2.81	2.89	2.87
Ho	0.72	0.84	0.83	0.75	0.66	0.99	0.68	0.70	0.72
La	11.7	13.9	15.5	13.4	12.3	16.2	13.8	13.9	14.6
Lu	0.23	0.28	0.28	0.22	0.22	0.34	0.28	0.25	0.27
Nb	3.77	3.82	6.00	4.53	3.87	4.71	4.37	4.52	4.83
Nd	14	16.5	17.6	15.3	14.1	18.9	15.4	15.8	16.4
Pr	2.94	3.61	4.11	3.68	3.44	4.53	3.77	3.84	4.08
Rb	22.9	29.5	24.7	26.6	24.3	25.5	30.1	28.7	29.8
Sm	3.37	3.39	4.27	3.43	3.28	4.73	3.45	3.60	3.62
Sn	0.9	2.7	0.6	1.4	0.6	0.5	0.6	0.7	0.7
Sr	195	210	225	198	193.0	210	234	231	216
Ta	0.2	0.2	0.2	0.2	0.1	0.2	0.2	0.2	0.2
Tb	0.51	0.64	0.62	0.59	0.49	0.78	0.52	0.55	0.59
Th	1.76	1.84	2.12	2.05	1.78	2.02	2.03	2.23	2.32
Tm	0.27	0.3	0.32	0.26	0.26	0.38	0.26	0.29	0.29
U	2.16	2.87	0.42	2.96	0.41	0.42	0.49	0.53	0.55
V	248	239	223	221	218	229	219	231	228
W	0.5	<0.5	0.6	<0.5	0.5	0.5	<0.5	0.6	1.0
Y	16.5	22.5	25.6	19.3	17.3	31.5	17.9	18.6	19.1
Yb	1.65	1.98	1.93	1.69	1.71	2.26	1.69	1.75	1.81
Zr	88	95	101	102	97	106	104	107	116
Th_N/ Nb_N	3.91	4.03	2.96	3.79	3.85	3.59	3.9	4.13	4.03
Th_N/ La_N	1.21	1.07	1.11	1.23	1.16	1.00	1.19	1.29	1.28
Lan/ Yb_n	4.78	4.73	5.41	5.35	4.85	4.83	5.51	5.36	5.44
Ce_n/ Yb_n	3.79	3.55	4.26	4.1	4.1	3.49	4.59	4.55	4.6
Ta_N/La_N	0.29	0.24	0.32	0.25	0.14	0.21	0.33	0.24	0.23
Hf_N/Sm_N	1.06	1.12	1.17	1.21	1.07	0.8	1	1.15	1.14
Eu/Eu*	0.81	0.93	0.85	0.82	0.92	0.79	0.9	0.91	0.87

DI: Q+Fk+Ab+Ne+Leu is calculated from CIPW normative percentage, after Thornton *et al.* (1960) (Q = quartz, Fk = orthoclase, Ab = albite, Ne = nepheline, Leu = leucite), $Eu/Eu^* = Eu_n/((Gd_n + Sm_n)/2)$: standard formula for calculated Eu anomalies.

microphotographs in Figures 3 and 4 through uralitization of augite, biotite chloritization and ferro-edenite epidotization. In addition, the partially preserved ophitic textures of the Group II dykes and their higher proportions of late-magmatic (ferro-edenite, biotite) and secondary (chlorite and epidote) minerals also indicate the relative degree of hydrothermal or deuteric alteration in Group II dykes compared to Group I dykes. The presence of ferro-edenite and biotite at the margins of the large augite crystals is similar to deuteric alteration described in the Liptako area WNW-ESE to NW-SE trending doleritic dykes; suggesting the evolution of magma under variable fluid pressures, leading to interaction between crystals and hydrothermal aqueous fluids (Noura *et al.*, 2023a). In addition, LILE (K, Sr, Rb, Ba and Cs) and Na contents can be used to test hydrothermal alteration. When we examined the relative variation of Ba (272–751 ppm), Sr (195–234 ppm) and Cs

Table 7. Whole-rock major (wt%) and trace elements (ppm) compositions of Group II dykes. LOI = Loss On Ignition, N = primitive mantle, n = chondrite.

Samples	TD3a	TD4a	TD2a	TD2	TD3	TD4
Lat. N	14.288	14.273	14.271	14.271	14.288	14.273
Long. E	1.411	1.408	1.406	1.406	1.411	1.408
Major elements (wt%)						
SiO_2	55.9	54.7	56.6	56.6	54.8	56.5
Al_2O_3	12.85	13.05	13.2	13.1	12.75	12.35
Fe_2O_3	13.7	15.35	14.05	13.85	13.8	13.60
CaO	6.49	6.03	6.34	6.5	6.81	6.23
MgO	3.03	3.47	3.13	2.95	3.2	2.90
Na_2O	2.57	3.59	2.84	2.81	2.69	2.81
K_2O	1.68	0.93	1.52	1.62	1.62	1.58
Cr_2O_3	0.009	0.007	0.009	0.005	0.008	0.004
TiO_2	1.36	1.42	1.39	1.34	1.34	1.38
MnO	0.17	0.19	0.18	0.18	0.18	0.17
P_2O_5	0.21	0.21	0.23	0.22	0.2	0.23
SrO	0.03	0.02	0.03	0.03	0.03	0.03
BaO	0.06	0.05	0.07	0.05	0.04	0.05
LOI	1.99	2.22	2.34	1.75	1.88	1.78
Total	100.05	101.24	101.93	101.01	99.35	99.61
Mg#	33.20	33.69	33.37	32.38	34.26	32.40
DI	36.15	22.81	48.96	49.28	46.53	50.00
Trace elements (ppm)						
Ba	569	423	616	439	411	442
Ce	49.1	41.4	46.1	45.2	43.4	48.2
Cr	66	51	63	41	60	34
Cs	0.95	0.4	0.86	1.2	1.42	1.25
Dy	5.44	5.08	5.09	5.1	5.01	5.10
Er	2.96	2.84	2.91	2.8	2.89	2.79
Eu	1.54	1.52	1.66	1.49	1.49	1.49
Ga	23.1	22.1	23.4	23.1	22.9	21.0
Gd	6.21	5.48	5.73	5.49	5.31	5.62
Hf	4.67	4.1	4.48	4.35	4.11	4.35
Ho	1.18	1.06	1.08	1.09	1.08	1.11
La	21.9	20	22.2	21.3	20.3	21.7
Lu	0.35	0.33	0.41	0.36	0.38	0.36
Nb	7.58	6.37	7.19	7.06	6.7	6.75
Nd	27.3	22.9	24.7	24.7	23.3	25.2
Pr	6.38	5.35	5.89	5.61	5.3	5.95
Rb	52.9	22.2	41.7	48	49.6	52.5
Sm	5.91	5.77	6.31	5.48	5.63	5.67
Sn	10.4	1.7	7.4	2.5	13	1.3
Sr	309	208	269	246	282	265
Ta	0.5	0.4	0.5	0.5	0.5	0.4
Tb	0.97	0.86	0.88	0.84	0.87	0.88
Th	3.78	3.25	3.77	3.76	3.48	3.65
Tm	0.44	0.39	0.41	0.44	0.41	0.39
U	3.34	2.08	1.96	2.11	1.5	1.25
V	341	394	352	339	362	312
W	0.9	0.7	1	1	0.9	0.9
Y	28.9	28.5	28.7	27.3	26.4	28.8
Yb	2.87	2.4	2.41	2.58	2.47	2.52
Zr	175	152	167	163	158	165
Th_N/ Nb_N	4.18	4.28	4.39	4.46	4.35	4.53

Table 7. (continued).

Samples	TD3a	TD4a	TD2a	TD2	TD3	TD4
Th_N/ La_N	1.39	1.31	1.37	1.42	1.38	1.35
La_n/ Yb_n	5.14	5.62	6.21	5.57	5.54	5.81
Ce_n/ Yb_n	2.33	4.46	2.21	2.44	2.27	2.41
Ta_N/La_N	0.38	0.34	0.38	0.39	0.41	0.31
Hf_N/Sm_N	1.14	1.02	1.02	1.14	1.05	1.1
Eu/Eu*	0.78	0.83	0.84	0.83	0.83	0.81

DI: Q+Fk+Ab+Ne+Leu is calculated from CIPW normative percentage, after Thornton *et al.* (1960) (Q = quartz, Fk = orthoclase, Ab = albite, Ne = nepheline, Leu = leucite), $Eu/Eu^* = Eu_n/((Gd_n + Sm_n)/2)$: standard formula for calculated Eu anomalies.

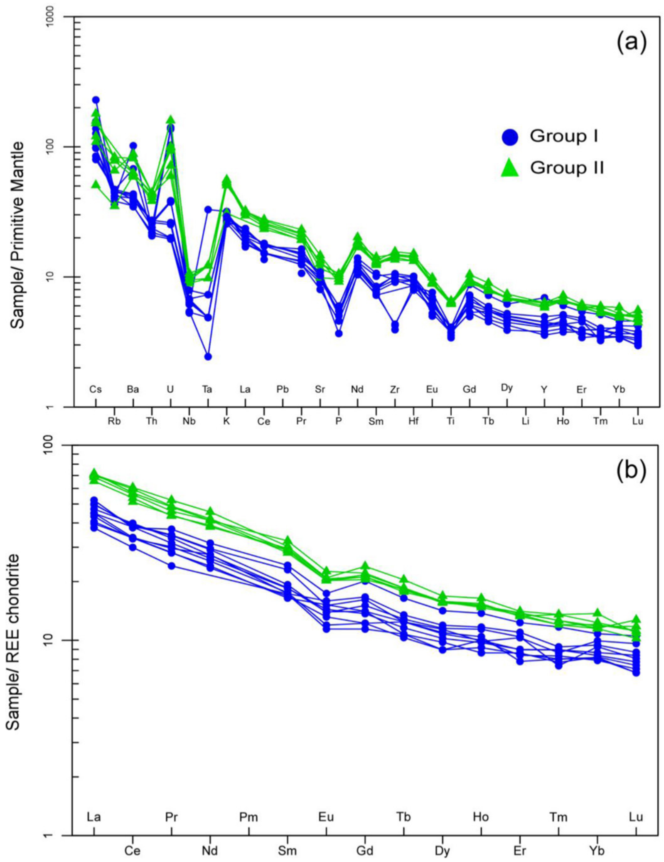

Fig. 7. (a) Extended primitive mantle normalized trace-element plot and (b) chondrite normalized REE plot for both groups. Primitive mantle normalizing values are from Sun and McDonough (1989) and chondrite normalizing values are from Boynton (1984). Blue and green symbols correspond to groups I and II, respectively.

(0.63–1.09 ppm) contents in Group I dykes compare to Group II dykes (Ba: 411–616 ppm, Sr: 208–309 ppm, Cs: 0.4–1.42 ppm), it seems that Group II dykes are slightly more affected by hydrothermal alteration. According to Backman *et al.* (1988), in presence of hydrothermal alteration, geochemical changes can be reflected in the variability of Rb contents within the rock groups. Rb contents in Group I dykes (Rb: 22.9–30.1 ppm) and in Group II dykes (Rb: 22.2–52.9 ppm) indicate the same evolution. Although hydrothermal or deuteric alteration was more important in Group II dykes than in Group I dykes and represented one of the important criteria for identifying the two groups, REE patterns indicate that it did not significantly affect the geochemical signature of the dykes in either group.

5.2 Magma genesis

5.2.1 Magma source

The Th/Ta ratio (6.96–17.8) obtained from both dyke groups of the Libiri swarm are typical of orogenic basalts (Th/Ta > 5, Cabanis and Thieblemont, 1988). In the Th/Nb *vs.* TiO_2/Yb (Pearce *et al.*, 2021) diagrams, the samples fall in the subduction zone field (Fig. 9). It should be emphasised that, even if these rocks project into the orogenic domain, they may also correspond to continental tholeiites. This is supported by the Y/Nb (3.64–4.47) ratios of 13 samples, which are typical of continental tholeiites (Y/Nb < 5, Winchester et Floyd, 1975). The SZLM (subduction-modified lithospheric mantle) fields correspond, according to these authors, to magmatic sources originating in the lithospheric mantle modified by subduction components. The Libiri NNW-NNE doleritic dyke swarm either originated from subduction zone activity or inherited such a context from the source. The fact that the dykes cannot be emplaced in an orogenic context (Noura *et al.*, 2023a) leads us to conclude that the source of these dykes is probably lithospheric mantle which had been metasomatized during earlier subduction zone associated with emplacement of Birimian rocks. This is evident when we consider the important negative Nb anomaly in the mantle-normalized trace-element spectra (Fig. 7a) and the slight slope in the Ti-Yb segment. The La_n/Yb_n ratio (4.73–5.81) in Group I and La_n/Yb_n (5.14–6.21) in Group II are essentially typical to those of garnet lherzolite sources ($La_n/Yb_n > 5$, McDonough & Sun, 1995; Oinam *et al.*, 2020). However, if melting of hydrated spinel lherzolite is also considered then Group I and Group II melts could have been sourced from partial melting of hydrated spinel or garnet lherzolite, at depths between 60 km to over 120 km in the mechanical lithosphere (Griffin *et al.*, 2009).

5.2.2 Magma evolution

The Mg# parameter and the DI (differentiation index) (Quartz + Alkali Feldspar + Albite + Nepheline + Leucite, Thornton *et al.*, 1960) are good indicators to test the basaltic magma evolution during its ascent (Ahmed *et al.*, 2018; Vicat

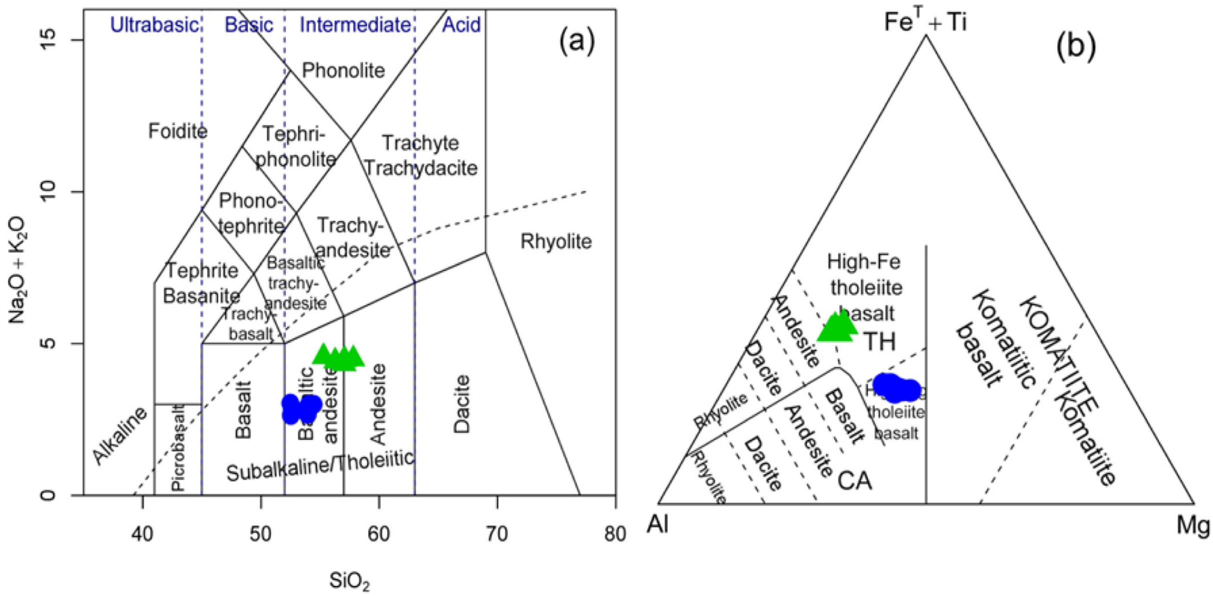

Fig. 8. (a) Total-alkali silica (TAS) (Le Bas *et al.*, 1986) and (b) Al-Fe^T+Ti-Mg (Jensen, 1976) classification diagrams showing tholeiitic nature of dykes in both groups. Symbols with blue circles belonging to Group I and green triangles belonging to Group II.

et al., 2001). Variation in Mg# and DI reflect magma that has evolved slightly between the two groups (*c.f.* Cox, 1980 and Vicat *et al.*, 1997) with Group I magma being more primitive (DI = 16.26–20.19, Mg# = 55–65) and Group II being more evolved (DI = 22.82–50.00, Mg# = 30–35). This interpretation is also support by SiO_2 contents which are relatively low in Group I dykes (51.0–54.2 wt%) and higher in Group II dykes (54.7–56.6 wt%) and the presence of more calcic-plagioclase in Group I dykes relative to Group II dykes. This difference can be associated to fractional crystallization or magma contamination by felsic rocks for Group II dykes. The relatively high (1.34–1.38 wt%) and low (0.74–0.89 wt%) TiO_2 contents in both Group are common to differentiated low-Ti basalts (TiO_2 < 2.5, Hou *et al.*, 2011) and continental LIPs described in Ernst *et al.* (2021), Pearce *et al.* (2021).

The Th/Ta and La/Yb ratios, which can be used to test crustal contamination (Condie, 1997), show higher values in Group I dykes (Th/Ta = 8.80–17.8, La/Yb = 7.02–8.17) relative to Group II dykes (Th/Ta = 6.96–9.26, La/Yb = 7.63–9.21). Similar ratio values, obtained by Tapsoba *et al.* (2018) on doleritic dykes in Burkina Faso (Th/Ta = 1.31–11.44 and La/Yb = 1.83–12.72), reflect magma contamination by the medium and upper continental crust. In the Ta_N/La_N *vs.* Hf_N/Sm_N (La Fleche *et al.*, 1998) and Nb/U *vs.* $(Th/Nb)_N$ (Panda *et al.*, 2023) diagrams, sample projections indicate metasomatism of the source by subduction-related processes (Fig. 10a) and magma contamination by the middle crust (Fig. 10b). According to these authors, the $(Th/Nb)_N$, Ta_N/La_N and Hf_N/Sm_N ratios were calculated relative to the primitive mantle of McDonough & Sun (1995). Both processes are also distinguished on the primitive mantle-normalized diagram by K and U enrichment and Nb depletion, typical of continental crust contaminants (Dupuy and Dostal, 1984; Rudnick and Gao, 2003). Furthermore, samples belonging to both groups have Th/Nb (0.38–0.54) and Th/La (0.13–0.17) ratios below the values normalized to the primitive mantle (Th_N/Nb_N = 3.25–4.58 and Th_N/La_N = 1.07–1.43),

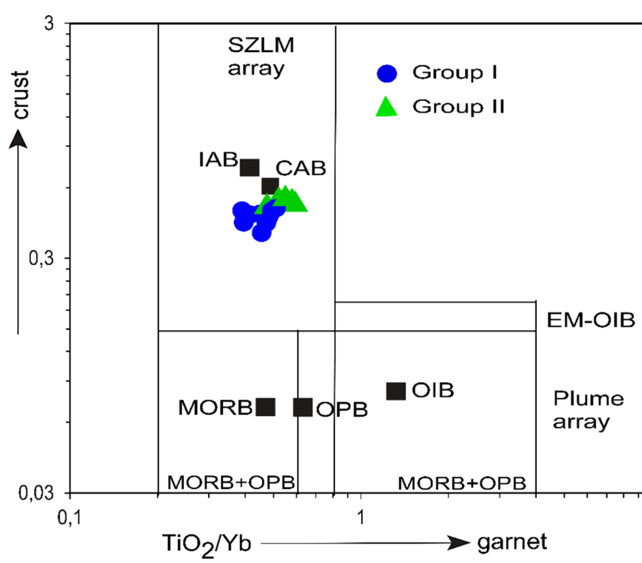

Fig. 9. Diagram Th/Nb *vs.* TiO_2/Yb (Pearce *et al.*, 2021) showing an inherited lithospheric modified mantle by subduction components origin of the dykes in both groups. SZLM = Subduction-modified lithospheric mantle, OIB = Oceanic Island basalts, OPB: Oceanic plateau basalts, MORB= Mid-ocean ridge basalts. Blue and green symbols correspond to groups I and II, respectively.

Tables 6 and 7. This behavior reflects a depletion in Nb relative to Th, which is typical of variable crustal contamination that occurred during interaction between crystals and late-magmatic fluid in the deeper magma chamber (Noura *et al.*, 2023a) or magma generated from a lithosphere that had been metasomatized during a prior subduction event (*c.f.* Pearce *et al.*, 2021). The simple projections in these diagrams and the low variation of La/Nb rations values from 2.75–3.63 in Group I dykes

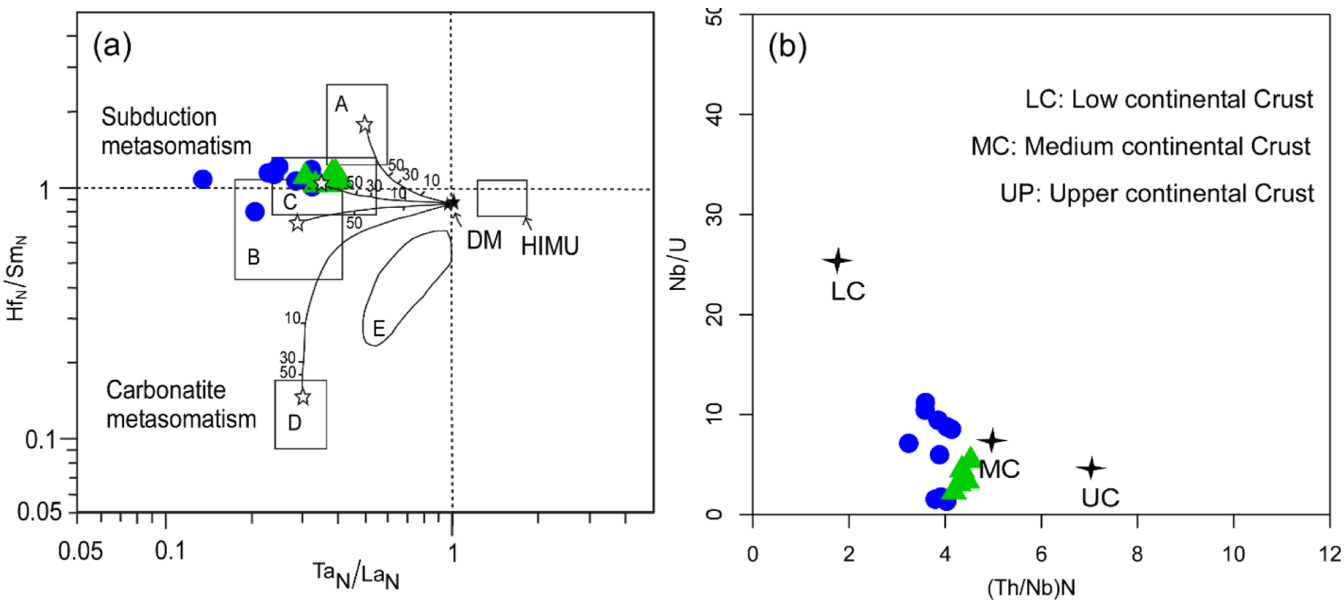

Fig. 10. (a) Ta_N/La_N *vs.* Hf_N/Sm_N (La Fleche *et al.*, 1998), (b) Nb/U *vs.* $(Th/Nb)_N$ (Panda *et al.*, 2023) diagrams showing the source of contamination. A, B, C: mantle sources metasomatized by subduction-related processes. D, E: mantle sources with carbonatite metasomatism. N = primitive mantle. Blue and green symbols correspond to groups I and II, respectively.

to 2.88–3.21 in Group II dykes suggest that *in situ* contamination has played a very minor role in distinguishing the two groups.

5.3 Geodynamic setting

The geodynamic setting of mafic rocks can be interpreted by using high field strength elements which resist low-grade metamorphic processes (Th, Nb, Hf, Zr, Ti, Ta, Yb, Pearce and Cann, 1973; Wood, 1980). On the Th/Yb *vs.* Ta/Yb diagram (Pearce, 1982), sample projection suggests that both groups derive from an island arc setting (Fig. 11b). These geotectonic settings have been reported by geochemical studies carried out on the Birimian (2.2–2.1 Ga) metabasalts of the Sirba (Ama Salah *et al.*, 1996) and Diagorou-Darbani belts (Soumaila *et al.*, 2004; Soumaila *et al.*, 2016a), the granitoids of the Gorouol belt (Hallarou, 2021) and the anorthosites of the Makalondi belt (Garba Saley, 2022). By extension, juvenile and mature volcanic oceanic shelf and island arc contexts have been described for other Birimian rocks elsewhere in the West African Craton (Asiedu *et al.*, 2004; Augustin and Gaboury, 2017; Baratoux *et al.*, 2011; Béziat *et al.*, 2000; Dampare *et al.*, 2008; De Kock *et al.*, 2011; Grenholm *et al.*, 2019; Lompo, 2009; Sakyi *et al.*, 2020; Senyah *et al.*, 2016). Thus, the basaltic andesite characteristics presented by these doleritic dykes can be explained by involvement of melts derived from a lithospheric mantle modified by older subduction of Birimian rocks.

Given the U-Pb age of 1791 ± 3 Ma (Baratoux *et al.*, 2019) on the SD dyke of our NNW-NNE doleritic dykes, we can infer that Libiri swarm postdates the end of the Eburnean orogeny around 1800 Ma (Bonhomme, 1962) and would indicate that metasomatism of the lithospheric mantle could have been caused by this phenomena. Additional U-Pb dating of the

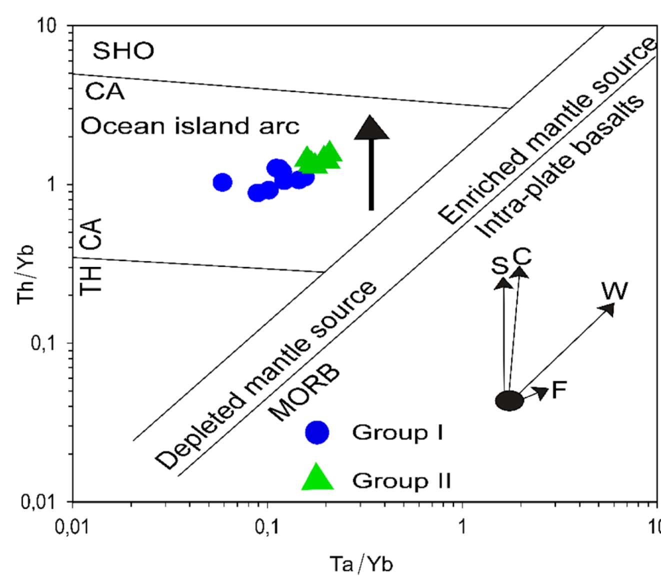

Fig. 11. Diagram Th/Yb *vs.* Ta/Yb (Pearce, 1982) showing the geodynamic setting of the NNW-NNE Libiri swarm. Th = Tholeiitic, CA = Calc-alkaline, SHO = Shoshonitic, MORB= Mid- Ocean ridge basalts. Blue and green symbols correspond to groups I and II, respectively.

NNW-NNE dykes will be important to confirm the 1791 Ma age for the NNW-NNE swarm as a whole.

Baratoux *et al.* (2019) offer a reconstruction which combines the 1791 Ma Libiri dyke with coeval dykes (1780–1790 Ma) in Sarmatia portion of Baltica (*e.g.*, Bogdanova *et al.*, 2013; Shumlyanskyy *et al.*, 2016) and Amazonia (Norcross *et al.*, 2000; Reis *et al.*, 2022; Santos *et al.*, 2002), and show an overall radiating swarm focused on the Libiri swarm region. The establishment of the Libiri swarm was linked according to Baratoux *et al.* (2019) to a major mantle plume.

6 Conclusion

The mineralogical and geochemical results demonstrate that the NNW-NNE doleritic dyke swarm in the Liptako region of Niger, consists of evolved tholeiitic basalts. Given the match of the SD sample, collected at the same site as the sample dated at 1791 ± 3 Ma from the Libiri pit of the Samira gold mine (Baratoux *et al.*, 2019), we propose that these dykes collectively represent the 1791 Ma Libiri dyke swarm which was emplaced c. 100–150 myr after the end of the Eburnean orogeny and have inherited the geochemical signature of lithospheric mantle which had been metasomatized by Eburnean subduction. The upwelling of magma in a post-orogenic context is linked to the arrival of mantle plume and interpretation of the swarm as part of a broad 1790 Ma Large Igneous Province present in the West African craton, formerly adjacent Sarmatia (part of Baltica) and Amazonia. Two geochemical groups can be distinguished in the 1790 Ma Libiri swarm. These groups differ notably in terms of their SiO_2 content, as well as the Mg# and An# of their plagioclase. However, their similar REE slopes suggest that Group II rocks are more evolved than Group I rocks. Group II rocks being characterised by greater alteration than Group I rocks. However, it should be noted that this alteration only affects the macroscopic appearance of the rocks. Interestingly, from a geochemical point of view, Group II rocks appear to be less affected by alteration than Group I rocks. The presence of late-magmatic hydrous minerals (ferro-edenite, biotite), whose proportion varies between the two groups, reflects the evolution of magma under variable fluid pressures and their interaction with early formed large crystals. The evolution of mineral phases is reflected by significant chemical zonation between the cores and margins of plagioclase and augite and the development of late-magmatic hydrous and hydrothermal alterations or post-magmatic metamorphism minerals on the margins.

Acknowledgments

The present work has also benefited from support from Dr. Philippe de Parseval for the microprobe analyses. We thank Mohamed Pegnalogo Ouattara from the UFR SRTM UFHB laboratory for the preparation of the thin sections.

Funding

The geochemistry analyses were funded by the Large Igneous Province (LIPs) project led by Dr. Richard E. Ernst, “LIPs-Industry Consortium for Resource Exploration (with Industry funding matched by Canadian NSERC grant CRDPJ523131-17; www.supercontinent.org).

References

Abdou A, Bonnot H, Bory Kadey D, Chalamet D, Saint Martin M, Younfa I. 1998. Notice explicative des cartes géologiques du liptako à 1/100000e et 1/200 000e. *Ministère Des Mines et de la Géologie, République du Niger,* Niamey, 64.

ACDI. 1973. Levé aéromagnétique du Liptako Gourma. *Ministère Des Mines et de l'Energie, Niamey, République Du Niger.*

Ahmed Y, Attourabi SA, Hallarou MM, Chamsi LI, Noura GR, Sanda CMM. 2022. Relationship between regional deformation and the emplacement of the Dibilo pegmatites (Liptako, West Niger). *J Afr Earth Sci* 198: 1–16.

Ahmed Y, Soumaila A, Harouna M. 2018. Basaltes quaternaires du Fossé de Termit-Agadem (Niger Oriental): caractérisation et signification géodynamique. Annal Univ Abdou Moumouni, Tome XXIII-A, 1: 91–111.

Affaton P, Gaviglio P, Pharisat A. 2000. Réactivation du craton ouest-africain au Panafricain: Paléocontraintes déduites de la fracturation des grès néoprotérozoïques de Karey Gorou (Niger, Afrique de l'Ouest). *Comptes Rendus de l'Academie de Sciences – Serie IIa: Sciences de La Terre et Des Planetes* 332: 609–614.

Aifa T, Lefort JP, Drareni A. 2001. When did the India – Asia collision really happen? *Gondwana Res* 4: 559–560.

Ama Salah I, Liegeois JP, Pouclet A. 1996. Evolution d'un arc insulaire océanique birimien précoce au Liptako nigérien (Sirba): Géologie, géochronologie et géochimie. *J Afr Earth Sci* 22: 235–254.

Ama Salah I. 1991. Pétrographie et relations structurales des formations metavolcaniques et sédimentaires du Birimien du Niger occidental. Problème de l'accrétion crustale au paléoprotérozoique inférieur. *Thèse de Doctorat de l'Université d'Orléan*, 270p.

Asiedu DK, Dampare SB, Sakyi PA, Banoeng-Yakubo B, Osae S, Nyarko BJB, *et al.* 2004. Geochemistry of Paleoproterozoic metasedimentary rocks from the Birim diamondiferous field, southern Ghana: Implications for provenance and crustal evolution at the Archean-Proterozoic boundary. *Geochem J* 38: 215–228.

Attourabi S, Marieke VL, Hallarou MM, Ahmed A, Mamane Moustapha Y, Chékaraou S. 2024b. Petrogragenetic realtionships between paleoproterozoic granitoids and rare-element pegmatites from Dibilo (Liptako, West Niger, West African Craton). *J Afr Earth Sci* 220: 105440.

Augustin J, Gaboury D. 2017. Paleoproterozoic plume-related basaltic rocks in the Mana gold district in western Burkina Faso, West Africa: Implications for exploration and the source of gold in orogenic deposits. *J Afr Earth Sci* 129: 17–30.

Backman JDRA, *et al.* 1988. Proc. ODP, Init. Repts 115 College Station, TX (Ocean Drilling Program). Proceedings of the Ocean Drilling Program, 115 Initial Reports.

Baratoux L, Metelka V, Naba S, Jessell MW, Grégoire M, Ganne J. 2011. Juvenile Paleoproterozoic crust evolution during the Eburnean orogeny (~2.2-2.0Ga), western Burkina Faso. *Precambrian Res* 191: 18–45.

Baratoux L, Söderlund U, Ernst RE, Roever E, Jessell MW, Kamo S, *et al.* 2019. New U-PB baddeleyite ages of mafic dyke swarms of the west African and amazonian cratons: Implication for their configuration in supercontinents through time. *Springer Geol* 263–314.

Bassot J-P., Cantagrel J-M., Jamond C. 1986. Nouvelles données géochronologiques sur les dolérites et gabbros de l'est du Sénégal et de la Guinée Bisseau. Reflexions sur l'age de mise en place et la répartition du magmatisme tholéiitique continental à l'échelle de l'Afrique de l'Ouest. *CNRS, UA, Université de Clermont II, France* 7: 1–14.

Béziat D, Bourges F, Debat P, Lompo M, Martin F, Tollon F. 2000. A Paleoproterozoic ultramafic-mafic assemblage and associated volcanic rocks of the Boromo greenstone belt: Fractionates originating from island-arc volcanic activity in the West African craton. *Precambrian Res* 101: 25–47.

Bogdanova VS, Gintov OB, Kurlovich DM, Lubnina NB, Nilsson MKM, Orlyuk MI, *et al.* 2013. Late Palaeoproterozoic mafic dyking in the Ukrainian Shield of Volgo-Sarmatia caused by rotation during the assembly of supercontinent Columbia (Nuna). *Lithos* 12: 196–216.

Bonhomme M. 1962. Contribution à l'étude géochronologique de la plate-forme de l'Ouest Africain. *Annals de la Faculté des Sciences de Université de Clermont-Ferrand Géol. Minéral* 5: 62.

Boynton WV. 1983. Cosmochemistry of the rare earth elements: meteorite studies. *Rare Earth Element Geochem* 63–114.

Bryan SE, Ferrari L. 2013. Large igneous provinces and silicic large igneous provinces: Progress in our understanding over the last 25 years. *Bull Geol Soc Am* 125: 1053–1078.

Cabanis B, Thieblemont D. 1988. La discrimination des tholeiites continentales et des basaltes arriere-arc; proposition d'un nouveau diagramme, le triangle Th-3xTb-2xTa. *Bulletin de La Société Géologique de France* 6: 927–935.

Chabou MC, Bertrand H, Sebaï A. 2010. Geochemistry of the Central Atlantic Magmatic Province (CAMP) in south-western Algeria. *J Afr Earth Sci* 58: 211–219.

Chabou MC, Sebai A, Féraud G, Bertrand H. 2007. Datation Ar / 39 Ar de la province magmatique de l ' Atlantique central dans le Sud-Ouest algérien. *Comptes Rendus Geosci* 339: 970–978.

Cheilletz A, Cuney M, ... B. C. 1994. 40 Ar/39 Ar ages of the Beauvoir topaze-lepidolite leucogranite and the Chedeville sodolithic pegmatite (North French Massif Central). Petrologic and geodynamic signfication. *CR Acad Sci Paris, t. 315, Série II*, 329–336.

Condie KC. 1997. Sources of proterozoic mafic dyke swarms: Constraints from Th/Ta and La/Yb ratios. *Precambrian Res* 81: 3–14.

Cournède C. 2010. Etude pétrographique, géochimique et paléo-magnétique de dykes doléritiques au Burkina Faso. MSc. Thesis, Univ. Toulouse. 32 p.

Cox KG. 1980. A model for flood basalt vulcanism. *J Petrol* 21: 629–650.

Dampare SB, Shibata T, Asiedu DK, Osae S, Banoeng-Yakubo B. 2008. Geochemistry of Paleoproterozoic metavolcanic rocks from the southern Ashanti volcanic belt, Ghana: Petrogenetic and tectonic setting implications. *Precambrian Res* 162: 403–423.

De Kock GS, Armstrong RA, Siegfried HP, Thomas E. 2011. Geochronology of the Birim Supergroup of the West African craton in the Wa-Bolé region of west-central Ghana: Implications for the stratigraphic framework. *J Afr Earth Sci* 59: 1–40.

Deer WA, Howie RA, Zussman J. 1986. An introduction to the rock-forming minerals, 17th ed. Longman Ltd., 528p.

Dupuis D, Pons J, Prost AE. 1991. Mise en place de plutons et caractérisation de la déformation au Niger Occidental. CR Acad Sci Paris, t.309, 816 Série ll, 1847–1853.

Dupuy C, Dostal J. 1984. Trace element geochemistry of some continental tholeiites. *Earth Planet Sci Lett* 67: 61–69.

Egal E, Thiéblemont D, Lahondère D, Guerrot C, Costea CA, Iliescu D, *et al.* 2002. Late Eburnean granitization and tectonics along the western and northwestern margin of the Archean Kénéma-Man domain (Guinea, West African Craton). *Precambrian Res* 117: 57–84.

El Bahat A, Ikenne M, Söderlund U, Cousens B, Youbi N, Ernst RE, *et al.* 2013. U-Pb baddeleyite ages and geochemistry of dolerite dykes in the Bas Drâa Inlier of the Anti-Atlas of Morocco: Newly identified 1380Ma event in the West African Craton. *Lithos* 174: 85–98.

Ernst RE, Bond DPG, Zhang SH, Buchan KL, Grasby SE, Youbi N, *et al.* 2021. Large igneous province record through time and implications for secular environmental changes and geological time-scale boundaries. In Large Igneous Provinces: A Driver of Global Environmental and Biotic Changes 26p.

Ernst RE, Bleeker W, Söderlund U, Kerr AC. 2013. Large Igneous Provinces and supercontinents: Toward completing the plate tectonic revolution. *Lithos* 174: 1–14.

Ernst RE, Buchan KL. 2002. Maximum size and distribution in time and space of mantle plumes: evidence from large igneous provinces. *J Geodyn* 34: 309–342.

Garba Saley H, Konaté M, Okunlola OA. 2024. Petrographic study of mn-bearing gondite (Birimian) of téra area in the leo-man shield (West African Craton) in Niger. *Econ Environ Geol* 57: 25–39.

Garba Saley H. 2022. Contexte de mise en place des minéralisations en chrome et en cuivre des formations birimièennes de la région de Makalondi (Liptako, Ouest Niger): implication géodynamique. Thèse de Doctorat de l'Université Abdou Moumouni de Niamey, 260p.

Gasquet D, Barbey P, Adou M, Paquette JL. 2003. Structure, Sr-Nd isotope geochemistry and zircon U-Pb geochronology of the granitoids of the Dabakala area (Côte d'Ivoire): Evidence for a 2.3 Ga crustal growth event in the Palaeoproterozoic of West Africa? *Precambrian Res* 127: 329–354.

Grenholm M, Jessell M, Thébaud N. 2019. A geodynamic model for the Paleoproterozoic (ca. 2. 27–1.96 Ga) Birimian Orogen of the southern West African Craton – Insights into an evolving accretionary-collisional orogenic system. *Earth-Sci Rev* 192: 138–193.

Griffin WL, O'Reilly SY, Afonso JC, Begg GC. 2009. The composition and evolution of lithospheric mantle: A re-evaluation and its tectonic implications. *J Petrol* 50: 1185–1204.

Grill R. 2010. Igneous rocks and processes: a practical guide. Chichester, UK: Wiley-Blackwell, p. 440.

Hafid A, Sagon JP, Julivert M, Arboleya ML, Saquaque A, El-Boukhari A, *et al.* 2001. Neoproterozoic basic dykes of the Zenaga Inlier, central Anti-Atlas, Morocco: Petrology, geochemistry and geodynamic significance. *J Afr Earth Sci* 32: 707–721.

Hallarou MM, Konaté M, Olatunji AS, Ahmed Y. 2020b. The Kourki porphyry Cu-Mo deposit is located in the southern part of the Gorouol greenstone belt in Western. *Geol Soc London Spec Publ* 1: 1–13.

Hallarou MM. 2021. Contexte de mise en place des minéralisations en cuivre et en molybdène des formations birimiennes de la région de Kourki (Liptako, Ouest Niger): Génèse et évolution magmatique. Thèse de Doctorat, Université Abdou Moumouni de Niamey, 255p.

Hirdes W, Davis DW. 2002. U-Pb geochronology of Paleoproterozoic rocks in the southern part of the Kedougou-Kéniéba Inlier, Senegal, West Africa: Evidence for diachronous accretionary development of the Eburnean province. *Precambrian Res* 118: 83–99.

Hou, T., Zhang, Z., Kusky, T., Du, Y., Liu, J., Zhao, Z. (2011). A reappraisal of the high-Ti and low-Ti classification of basalts and petrogeneticlinkage between basalts and mafic–ultramafic intrusions in the Emeishan Large gneous Province, SW China.Ore Geology Reviews 41, 133–143

Jensen LS. 1976. A new plot for classifying subalkalic volcanic rocks. *Ontario Division of Mines, Miscellaneous, Paper* 66: 1–2.

Jessell M, Santoul J, Baratoux L, Youbi N, Ernst RE, Metelka V, *et al.* 2015. An updated map of West African mafic dykes. *J Afr Earth Sci* 112: 440–450.

Koffi AY, Thébaud N, Kouamelan AN, Baratoux L, Bruguier O, Vanderhaeghe O, *et al.* 2022. Archean to Paleoproterozoic crustal evolution in the Sassandra-Cavally domain (Côte d'Ivoire, West Africa): Insights from Hf and U-Pb zircon analyses. *Precambrian Res* 382: 1–23.

Kouamelan AN, Kra KSA, Djro SC, Paquette JL, Peucat JJ. 2018. The Logoualé Band: A large Archean crustal block in the Kenema-Man domain (Man-Leo rise, West African Craton) remobilized during Eburnean orogeny (2.05 Ga). *J Afr Earth Sci* 148: 6–13.

Kouyaté D, Söderlund U, Youbi N, Ernst RE, Ha A, Ikenne M, *et al.* 2013. Lithos U – Pb baddeleyite and zircon ages of 2040 Ma, 1650 Ma and 885 Ma on dolerites in the West African Craton (Anti-Atlas inliers): Possible links to break-up of Precambrian supercontinents. *Lithos* 174: 71–84.

La Fleche MR, Camiré G, Jenner GA. 1998. Geochemistry of post-Acadian, Carboniferous continental intraplate basalts from the Maritimes Basin, Magdalen Islands, Quebec, Canada. *USDA Forest Service – General Technical Report RMRS-GTR* 148: 115–136.

Lama C. 1993. Apport de la méthode K-Ar à la compréhension de l'histoire géologique des granitoïdes birimiens du Liptako (Niger Occidental) et des leucogranites à deux micas de Tagragra d'AKKA (Anti-Atlas Occidental, Maroc). Thèse INPN l'Université de Loraine, 142p.

Leake BE, Woolley AR, B. W. D. *et al.* 1997. Nomencalture of amphiboles: Report of the subcommittee on amphiboles of the international mineralogical association, commission on new minerals and mineral names. *Can Mineral* 35: 219–246.

Le Bas MJ, Le Maitre RW, Streckeisen A, Zanettin B. 1986. A chemical classification of volcanic rocks based on the total alkali-silica diagram. *J Petrol* 27: 745–750.

Lefort JP, Aifa T. 2001. Paleomagnetic and geochronological evidence for a large rotation of the West African craton between 1.9 and 1.4 Ga: A kinematic model for the fragmentation of columbia and the accretion of Rodinia. *Gondwana Res* 4: 1994–1995.

Liégeois JP, Claessens W, Camara D, Klerkx J. 1991. Short-lived Eburnian orogeny in southern Mali. Geology, tectonics, U-Pb and Rb-Sr geochronology. *Precambrian Res* 50: 111–136.

Lompo M. 2009. Geodynamic evolution of the 2.25-2.0 Ga Palaeoproterozoic magmatic rocks in the Man-Leo shield of the West African Craton. A model of subsidence of an oceanic plateau. *Geol Soc Spec Publ* 323: 231–254.

Machens E. 1973. Contribution à l'étude des formations du socle cristallin et de la couverture sédimentaire de l'Ouest de la République du Niger. *In Mém. BRGM N°* 82.

Marcelot G, Maury RC, Lefevre C. 1983. Mineralogy of Erromango lavas (New Hebrides): Evidence of an early stage of fractionation in island arc basalts. *Lithos* 16: 135–151.

Marzoli A, Callegaro S, Dal Corso J, Davies JHFL, Chiaradia M, Youbi N, *et al.* 2018. The Central Atlantic Magmatic Province (CAMP): a review. In: Tanner LH, ed. The late triassic world: earth in a time of transition, topics in geobiology. Cham: Springer International Publishing, pp. 91–125.

McDonough, W. F., Sun, S. s. (1995). The composition of the Earth. Chemical Geology, 120(3–4), 223–253

Mottl MJ. 1983. Metabasalts, axial hot springs, and the structure of hydrothermal systems at mid-ocean ridges (Atlantic Ocean). *Geol Soc Am Bull* 94: 161–180.

Morimoto N, Fabries J, Ferguson AK, Ginzburg IV, Ross M, Seifert FA, *et al.* 1988. Nomenclature of pyroxenes. *Bulletin de Minéralogie* 111: 535–550.

Moutbir O, Aarab EM, Youbi N, Ait Lahna A, Tassinari CCG, Mata J, *et al.* 2024. Evidence of a large igneous province at ca. 347–330 Ma along the northern Gondwana margin linked to the assembly of Pangea: Insights from U-Pb zircon geochronology and geochemistry of the South-Western Branch of the Variscan Belt (Morocco). *Earth-Sci Rev* 258: 104905.

Naba S. 2007. Propriétés magnétiques et caractères structuraux des granites du Burkina Faso oriental (Craton Ouest Africain, 2,2-2,0 Ga): implications géodynamiques. Thèse de Doctorat de l'Université de Toulouse, 175p.

Norcross C, Davis DW, Spooner ETC, Rust A. 2000. U-Pb and Pb-Pb age constraints on Paleoproterozoic magmatism, deformation and gold mineralization in the Omai area, Guyana Shield. *Precambrian Res* 102: 69–86.

Noura GR, Ahmed Y, Baratoux L, Ernst RE, Attourabi SA, Hallarou MM, *et al.* 2023a. Petrogenesis and geochemistry of WNW-ESE to NW-SE trending doleritic dykes of the Paleoproterozoic Liptako basement (West African Craton, West Niger). *J Afr Earth Sci* 208: 1–17.

Oinam GS, Krishnakanta A, *et al.* 2020. Extension continentale de la marge septentrionale du Gondwana dans l ' Himalaya oriental: contraintes de la géochimie et des âges de zircon U – Pb des intrusifs Extension continentale de la marge septentrionale du Gondwana dans l ' Himalaya oriental: co. *Comptes Rendus Géoscience*, *Tome* 352: 19–41.

Parra-Avila LA, Kemp AIS, Fiorentini ML, Belousova E, Baratoux L, Block S, *et al.* 2017. The geochronological evolution of the Paleoproterozoic Baoulé-Mossi domain of the Southern West African Craton. *Precambrian Res* 300: 1–27.

Pawlig S, Gueye M, Klischies R, Schwarz S, Wemmer K, Siegesmund S. 2006. Geochemical and Sr-Nd isotopic data on the Birimian of the Kedougou-Kenieba Inlier (Eastern Senegal): Implications on the Palaeoproterozoic evolution of the West African Craton. *South Afr J Geol* 109: 411–427.

Pearce JA, Ernst RE, Peate DW, Rogers C. 2021. LIP printing: use of immobile element proxies to characterize Large Igneous Provinces in the geologic record. *Lithos* 392-393: 1–28.

Pearce JA. 1982. Trace element characteristics of lavas from destructive plate boundaries. In: Thorpe RS, ed. Andesite. Chichester: J. Wiley and Sons pp. 525–548.

Pearce JA, Cann JR. 1973. Tectonic setting of basic volcanic rocks determined using trace element analyses. *Earth Planet Sci Lett* 19: 290–300.

Panda A, Sarma DS, Patel R. 2023. Geochemistry, magma flow characteristics and petrogenesis of Paleoproterozoic NW-NNW trending mafic dykes from central Bastar craton, India. *J Earth Syst Sci* 132: 1–28.

Pons J, Barbey P, Dupuis D, Léger JM. 1995. Mechanisms of pluton emplacement and structural evolution of a 2.1 Ga juvenile continental crust: the Birimian of southwestern Niger. *Precambrian Res* 70: 281–301.

Porras MR. 2010. Genèse et évolution des magmas andésitiques à rhyodacitiques récents des volcans Misti et Ubinas (Sud du Pérou). Thèse de l'Université Blaise Pascal – Clermont Ferrand II, 409p.

Potrel A, Peucat JJ, Fanning CM. 1998. Archean crustal evolution of the West African Craton: example of the Amsaga Area (Reguibat Rise). U-Pb and Sm-Nd evidence for crustal growth and recycling. *Precambrian Res* 90: 107–117.

Reis NJ, Teixeira W, D'Agrella-Filho MS, Bettencourt JS, Ernst RE, Goulard LEA. 2022. Large igneous provinces of the Amazonian Craton and their metallogenic potential in Proterozoic times. In Srivastava RK, Ernst RE, Buchan KL, de Kock M, eds. Large Igneous Provinces and their Plumbing Systems. Geol Soc London Spec Publ 518: 493–529.

Rooney, A. D. Selby, D., Houzay, J. P., Renne, P. R. (2010). Re-Os geochronology of a Mesoproterozoic sedimentary succession, Taoudeni basin, Mauritania: Implications for basin-wide correlations and Re-Os organic-rich sediments systematics. Earth and Planetary Science Letters, 289: 486–496.

Rudnick RL, Gao S. 2003. Composition of the continental crust. *Treatise Geochem* 9: 1–64.

Santos JOS, Hartmann LA, McNaughton NJ, Fletcher IR. 2002. Timing of mafic magmatism in the Tapajós Province (Brazil) and implications for the evolution of the Amazon Craton: Evidence from baddeleyite and zircon U-Pb SHRIMP geochronology. *J South Am Earth Sci* 15: 409–429.

Sengupta P, Ray A, Pramanik S. 2014. Mineralogical and chemical characteristics of newer dolerite dyke around Keonjhar, Orissa: Implication for hydrothermal activity in subduction zone setting. *J Earth Syst Sci* 123: 887–904.

Sakyi PA, Su BX, Manu J, Kwayisi D, Anani CY, Alemayehu M, *et al.* 2020. Origin and tectonic significance of the metavolcanic rocks and mafic enclaves from the Palaeoproterozoic Birimian Terrane, SE West African Craton, Ghana. *Geol Mag* 157: 1349–1366.

Senyah GA, Dampare SB, Asiedu DK. 2016. Geochemistry and tectonic setting of the Paleoproterozoic metavolcanic rocks from the Chirano Gold District, Sefwi belt, Ghana. *J Afr Earth Sci* 122: 32–46.

Shumlyanskyy L, Ernst RE, Söderlund U, Billström K, Mitrokhin O, Tsymbal S. 2016. New U-Pb ages for mafic dykes in the Northwestern region of the Ukrainian shield: coeval tholeiitic and jotunitic magmatism. *GFF* 138: 79–85.

Söderlund U, Ernst RE, Youbi N, *et al.* 2013a. A major Archean (2688 Ma) dyke swarm discovered in the western Reguibat Shield, West African craton, Morocco. Unpublished Report #A131 (20 February 2013). *Consortium Project for Reconstruction of Supercontinents Supercontinents Back Back to 2.7 Ga Using t. Unpublished Report #A131 (20 February 2013)*. 6p

Soumaila A, Ahmed Y, Nouhou H. 2016b. Géochimie des basites et ultrabbasites de Ladanka (Liptako, Niger). *J Des Sci* 16: 37–54.

Soumaila A, Garba Z, Moussa IA, Nouhou H, Sebag D. 2016a. Highlighting the root of a paleoproterozoic oceanic arc in Liptako, Niger, West Africa. *J Geol Min Res* 8: 13–27.

Soumaila A, Henry P, Garba Z, Rossi M. 2008. REE patterns, Nd-Sm and U-Pb ages of the metamorphic rocks of the Diagorou-Darbani greenstone belt (Liptako, SW Niger): Implication for Birimian (Palaeoproterozoic) crustal genesis. *Geol Soc Spec Publ* 297: 19–32.

Soumaila A, Henry P, Rossy M. 2004. Contexte de mise en place des roches basiques de la ceinture de roches vertes birimienne de Diagorou-Darbani (Liptako, Niger, Afrique de l'Ouest): Plateau océanique ou environnement d'arc/bassin arrière-arc océanique. *Comptes Rendus Geoscience* 336: 1137–1147.

Soumaila A. 2000. Etude Structurale, pétrographique et géochimique de la ceinture Birimiènne de Diagorou Darbani, Liptako, Niger Occidental (Afrique de l'Ouest). Thèse de Doctorat de l'Université de France-Comté, 260p.

Speer JA. 1984. Micas in igneous rocks. In: Bailey SW, ed. Micas. Reviews in Mineralogy 13.

Sun SS, McDonough WF. 1989. Chemical and isotopic systematics of oceanic basalts: Implications for mantle composition and processes. *Geol Soc Spec Publ* 42: 313–345.

Tait J, Straathof G, Söderlund U, Ernst RE, Key R, Jowitt SM, *et al.* 2013. The ahmeyim great dyke of mauritania: a newly dated archaean intrusion. *Lithos* 174: 323–332.

Tapsoba BL, Ching-Hua H, Wenmenga U, Iizuka Y, Chung SL, Shellnutt G. 2018. Chemical and Sr-Nd compositions and 40Ar/39Ar ages of NW-trending dolerite dikes of Burkina Faso: Evidence for a Mesoproterozoic magmatism in the West African Craton. *Geosci Front* 9: 1957–1980.

Thiéblemont D, Goujou JC, Egal E, Cocherie A, Delor C, Lafon JM, *et al.* 2004. Archean evolution of the Leo Rise and its Eburnean reworking. *J Afr Earth Sci* 39: 97–104.

Thomas RJ, Chevallier LP, Gresse PG, Harmer RE, Eglington BM, Armstrong RA, *et al.* 2002. Precambrian evolution of the Sirwa Window, Anti-Atlas Orogen, Morocco. *Precambrian Res* 118: 1–57.

Traoré DY. 2017. Etude métallogénique du district aurifère de Syama (Mali): analyse comparative de gisements situés sur une même structure lithosphérique éburnéenne. Thèse de Doctorat de l'Université de Toulouse, pp. 40–75.

Thornton, et al. 1960. Chemistry of Igneous rocks I. Differentiation Index. *Am J Sci* 258: 664–684.

Vicat JP, Ngounouno I, Pouclet A. 2001. Existence de dykes doléritiques anciens à composition de tholéiites continentales au sein de la province alcaline de la ligne du Cameroun. Implication sur le contexte géodynamique. Comptes Rendus de l'Académie Des Sciences – Series IIA – *Earth Planet Sci* 332: 243–249.

Vicat JP, Pouclet A, Nkoumbou CM, Semé SA. 1997. The fissural Neoproterozoic volcanism of the Lower Dja, Yokadouma (Cameroon) and Nola (RCA) Series – Geotectonic meaning. *Comptes Rendus de l'Academie de Sciences – Serie IIa: Sciences de La Terre et Des Planetes* 325: 671–677.

Vidal M, Delor C, Pouclet A, Simeon Y, Alric G. 1996. Evolution géodynamique de l'Afrique de l'Ouest entre 2,2 Ga et 2 Ga: Le style «archéen» des ceintures vertes et des ensembles sédimentaires birimiens du nord-est de la Côte-d'Ivoire. *Bulletin de La Societe Geologique de France* 167: 307–319.

Vegas N, Naba S, Bouchez JL, Jessell M. 2008. Structure and emplacement of granite plutons in the Paleoproterozoic crust of Eastern Burkina Faso: Rheological implications. *Int J Earth Sci* 97: 1165–1180.

Verati C, Bertrand H, Féraud G. 2005. The farthest record of the Central Atlantic Magmatic Province into West Africa craton: Precise 40Ar/39Ar dating and geochemistry of Taoudenni basin intrusives (northern Mali). *Earth Planet Sci Lett* 235: 391–407.

Walsh GJ, Aleinikoff JN, Benziane F, Yazidi A, Armstrong TR. 2002. U-Pb zircon geochronology of the Paleoproterozoic Tagragra de Tata inlier and its Neoproterozoic cover, western Anti-Atlas, Morocco. *Precambrian Res* 117: 1–20.

Winchester JA, Floyd PA. 1975. Geochemical magma type discrimination application to altered and metamorphic basic igneous rocks. *Earth Planet Sci Lett* 28: 459–469.

Wood DA. 1980. The application of a Th–Hf–Ta diagram to problems of tectonomagmatic classification and to establishing the nature of crustal contamination of basaltic lavas of the British Tertiary Volcanic Province. *Earth Planet Sci Lett* 50: 11–30.

Youbi N, Ernst RE, Söderlund U, Boumehdi MA, Ait Lahna A, Tassinari CCG, *et al.* 2020. The Central Iapetus magmatic province: An updated review and link with the ca. 580 Ma Gaskiers glaciation. In Adatte T, Bond DPG, Keller G, eds. Mass

Extinctions, Volcanism, and Impacts: New Developments. Geol Soc Am Spec Paper 544: 35–66.

Youbi N, Kouyaté D, Söderlund U, Ernst RE, Soulaimani A, Hafid A, *et al.* 2013. The 1750 Ma magmatic event of the West African craton. *Precambrian Res* 236: 106–123.

Youbi N, Ernst R, Söderlund U, Bertrand H, Doblas M, El Hachimi H, *et al.* 2011. Large igneous provinces of the West African Craton: The record preserved in regional dyke swarms. Large Igneous Provinces Commision, May, 1–12.

Cite this article as: Noura GR, Baratoux L, Ernst RE, El Bilali H, Saley ALA, Hantchi KD, Bohari AD, Ahmed Y. 2025. Mineralogical and geochemical characteristics of the NNW-NNE trending Libiri doleritic dyke swarm of the Paleoproterozoic Liptako basement (West Niger): Genesis and magmatic evolution, *BSGF - Earth Sciences Bulletin* 196: 18. https://doi.org/10.1051/bsgf/2025019